Electronic Band Structure and Phase Transition in $TiCl_3$

Soichi Miyata

February 1978

Synopsis

Energy bands for the 3dε electrons of Ti^{3+} in the high temperature structure of $TiCl_3$ are calculated by the tight-binding approximation. Cubic symmetry around each Ti^{3+} is assumed and transfer between the 3p atomic orbitals of Cl^- and 3dε atomic orbitals of Ti^{3+} is considered. Two singlet bands and two doublet bands with no dispersion have been obtained. The dispersionless character is discussed by constructing Wannier functions. 3dε energy bands in the distorted structures of the Ti^{3+} lattice are also calculated. A distortion of the Ti^{3+} brings in a dispersion and an overlap of the bands through the intra-band mixing. For three types of distorted structure denoted as antidimerization, dimerization, and sheared structures, the electronic energy is found to be lowered. The relative stability at zero of temperature of these distorted structures is studied by comparing the total energy of the electron-lattice coupled system, and it is found that the antidimerization structure is the most stable. Self-consistency conditions to determine the chemical potential and the displacement of Ti ions at finite temperatures are derived in the mean field approximation. Temperature variation of the displacement and the transition temperature of the second order are calculated. The paramagnetic susceptibility is calculated on the basis of the obtained energy bands in both the undistorted and distorted structures. Possibility of superlattice structure and effects of the interband mixing are discussed.

Acknowledgements

The author would like to express his sincere gratitude to Professor K. Motizuki, under whose guidance this work was done, for valuable suggestions and enlightening discussions throughout the course of the work and also for her help in preparing the manuscript. Without her continuous encouragement and help, this work would not have been completed. He also thanks gratefully to Dr. N. Suzuki for stimulative discussions and helpful advice on computational calculations. Thanks are due to Miss T. Kimura for typing his thesis.

He would like to thank his wife, Mariko for continuous encouragement.

Contents

§1. Introduction

The α and γ modifications of $TiCl_3$ show a phase transition at 217 K as indicated by remarkable changes in the magnetic susceptibility,[1] lattice constants,[1] electrical conductivity,[2] and electronic absorption spectrum.[3] In their high temperature phase the Ti^{3+} ions form honeycomb lattices which intervene into the close-packed structure of the Cl^- ions, hexagonal close-packed in the α modification and cubic close-packed in the γ modification. The magnetic susceptibility observed by Ogawa[1] shows different temperature dependence above and below 217 K: in the high temperature range the susceptibility increases linearly with decreasing temperature and shows around 260 K a broad maximum, whereas below 217 K it decreases steeply and then shows a weak temperature dependence. Furthermore, the observed susceptibility is almost isotropic from 77 K to 370 K. No magnetic ordering was found by neutron diffraction experiment on the α-$TiCl_3$ powder sample at 4 K.[4] However, a recent experiment of far-infrared transmission at 80 K[4] indicates a lowering of crystal symmetry. These experimental results indicate that the phase transition is related to lattice distortion but not to magnetic ordering. In this paper we study theoretically what the nature of the phase transition really is.

As shown in §2 the two-dimensional energy bands for the 3dε electrons of Ti^{3+} in the high temperature phase have a special character. Two singlet bands and two doublet bands, all with no dispersion, are obtained. As a Ti^{3+} ion has one 3d electron and the unit cell of each layer contains two Ti^{3+} ions, the lowest singlet

band is fully occupied at 0 K by 3d electrons of up and down spins. A distortion of the Ti^{3+} lattice will, however, cause dispersion of each band as well as a splitting of each excited doublet band, and for large enough distortion an overlap of the bands may occur. When overlap occurs between the lowest band and the first excited band, electrons will be redistributed over the overlapped bands and the total electronic energy will be lowered. This decrease of energy may overcompensate the increase of the elastic lattice energy due to the distortion and may give a spontaneous distortion. Thermal excitation may then cause a phase transition to the undistorted lattice at a certain temperature.

In §2 energy bands for the 3dε electrons of Ti^{3+} in the high temperature structure of $TiCl_3$ are calculated by the tight-binding approximation. The dispersionless character is discussed by constructing Wannier functions. In §3 we calculate the energy bands in distorted structures of the Ti^{3+} lattice. Three types of distorted structure are considered which are called the antidimerization structure, the dimerization structure, and the sheared structure. In §4 the total energies (electronic energy + lattice energy) of the three distorted structures are calculated and by comparing them the most stable distorted structure at 0 K is determined. The self-consistent equations to determine both displacement of Ti ions and chemical potential at finite temperatures are derived and solved. In §5 the paramagnetic susceptibility is calculated for both the distorted and undistorted structures. In §6 discussions are given.

§2. Electronic Band Structure in Undistorted Lattice

2.1 Formulation

The crystal structures of the α and γ modifications of $TiCl_3$ are such that the Ti ions form honeycomb lattices which intervene into the colose-packed structure of the Cl^- ions, hexagonal close-packed in the α modification and cubic close-packed in the γ modification.(see Fig. 2-1) We take a unit sandwich structure out of the crystal of $TiCl_3$, which consists of one honeycomb lattice of Ti^{3+} and two close-packed Cl^- layers that enclose it from both sides. Each Ti^{3+} is surrounded by six Cl^- in octahedral configuration as shown in Fig. 2-2. The unit cell, defined by lattice vectors **a** and **b**, contains two Ti^{3+} (I and II) and six Cl^- (1,2,...,6). We consider only the low energy triplet state dε for Ti^{3+} in the cubic crystalline field and denote the three wave functions as ξ, η, ζ which are respectively of the yz, zx, xy types, the coordinate axes being the local cubic principal axes shown in Fig. 2-2. We construct tight-binding Bloch functions

$$\xi_\mu(r,k) = N^{-1/2} \sum_m \exp(ik\cdot R_{m\mu})\xi(r-R_{m\mu}), \text{ etc.,} \qquad (2.1)$$

where $R_{m\mu}$ is the position vector of the μth atom (μ=I,II) in the *m*th unit cell and N the number of unit cells. Similarly we construct Bloch functions from the 3p orbitals of the six Cl^- in the unit cell, $p_x(r-R_{m\mu})$, $p_y(r-R_{m\mu})$, $p_z(r-R_{m\mu})$, μ=1,2,...,6, as

$$p_{\mu x}(r,k) = N^{-1/2} \sum_m \exp(ik\cdot R_{m\mu})p_x(r-R_{m\mu}), \text{ etc..} \qquad (2.2)$$

Transfer integral and overlap integral for any pair out of these 24 Bloch functions will be assumed to arise only through nonorthogonal atomic orbitals, such as ζ of Ti^{3+}(I) and p_x of Cl^-(5), ζ of Ti^{3+}(II) and p_y of Cl^-(5), and either ξ of Ti^{3+}(I) or η of Ti^{3+}(II) and p_z of Cl^-(5). (see Fig. 2-3) All these nonorthogonal atomic orbitals give the same transfer integral γ and the same overlap integral S. We have only these two parameters γ and S in our calculation. Transfer and overlap between a p orbital of one Cl^- and another p orbital of an adjacent Cl^- will be neglected. The $d\varepsilon$ orbitals and the 3s or 4s orbital of a neighboring Cl^- are orthogonal, provided the cubic configuration of the atoms is exact,(*) so that we neglect s orbitals. Also, we do not consider 4p orbitals of Cl^- for the reason of their high energy. A deviation from cubic symmetry of the atomic arrangements will bring in small nonorthogonality for otherwise orthogonal atomic orbitals, but we shall not consider such a situation in the present study. Even with strict cubic symmetry of the atomic configuration, the layer structure of the crystal of $TiCl_3$ will give rise to a potential of noncubic symmetry which will produce a transfer integral between orthogonal atomic orbitals, if small, and also a splitting of the $d\varepsilon$ level.

(*) With the use of the lattice constants of $TiCl_3$ observed at room temperature the angle between two octahedral bonds, for example Ti(I)-Cl(5)-Ti(II), is estimated to be about 88° in both α- and γ-modifications.

All these will be neglected. Our treatment is in essence to take an antibonding molecular orbital for a Ti-3dε and the surrounding Cl-3p's to construct the 3d band (bonding molecular orbital if we consider the Cl-3p band).

Using 24 Bloch functions expressed by Eq. (2.1) and Eq. (2.2) we construct energy matrix H(k) and overlap matrix S(k). The band energy E is then obtained from the equation

$$\det|K(E,k)| \equiv \det|H(k) - ES(k)| = 0. \tag{2.3}$$

If we write

$$K(E,k) = \begin{pmatrix} K_{dd} & K_{dp} \\ K_{pd} & K_{pp} \end{pmatrix}, \tag{2.4}$$

then K_{dd} is a diagonal matrix of dimension 6 with equal diagonal elements $\varepsilon_d - E$, where ε_d is the energy of the dε level in the crystal. K_{pp} is also diagonal with equal diagonal elements $\varepsilon_p - E$. We write $\varepsilon_{dp}=\varepsilon_d-\varepsilon_p$ and set $\varepsilon_p=0$. Taking a matrix

$$A(E,k) = \begin{pmatrix} I & -K_{dd}^{-1}K_{dp} \\ -K_{pp}^{-1}K_{pd} & I \end{pmatrix}, \tag{2.5}$$

we have

$$K(E,k)A(E,k) = \begin{pmatrix} K_{dd}-K_{dp}K_{pp}^{-1}K_{pd} & 0 \\ 0 & K_{pp}-K_{pd}K_{dd}^{-1}K_{dp} \end{pmatrix}, \tag{2.6}$$

so that we have

$$\det|K_{dd}^{eff}| \equiv \det|K_{dd} - K_{dp}K_{pp}^{-1}K_{pd}| = 0. \tag{2.7}$$

The method used here is known as folding down of the secular equation. The effective matrix K_{dd}^{eff} is calculated to be

$$K_{dd}^{eff} = (\varepsilon_{dp} - E)I + x(E)\begin{pmatrix} 4 & 0 & 0 & 0 & e_1 & e_3 \\ 0 & 4 & 0 & e_1 & 0 & e_2 \\ 0 & 0 & 4 & e_3 & e_2 & 0 \\ 0 & e_1^* & e_3^* & 4 & 0 & 0 \\ e_1^* & 0 & e_2^* & 0 & 4 & 0 \\ e_3^* & e_2^* & 0 & 0 & 0 & 4 \end{pmatrix}, \tag{2.8}$$

where

$$x(E) = (\gamma - ES)^2/E, \qquad e_i = \exp(ik\cdot\tau_i), \tag{2.9}$$

τ_1, τ_2, τ_3 being vectors that join a Ti^{3+} to its three nearest neighbor Ti^{3+}'s (see Fig. 2-1). All e_i's in the matrix Eq. (2.8) will be replaced by 1 if we transform the matrix by a diagonal matrix of elements e_2^*, e_3^*, e_1^*, e_2, e_3, e_1, since $e_1e_2e_3=1$.
A further transformation by a unitary matrix

$$T = \frac{1}{\sqrt{6}} \begin{pmatrix} 1 & 1 & 1 & 1 & 1 & 1 \\ 1 & \omega & \omega^2 & 1 & \omega & \omega^2 \\ 1 & \omega^2 & \omega & 1 & \omega^2 & \omega \\ 1 & 1 & 1 & -1 & -1 & -1 \\ 1 & \omega & \omega^2 & -1 & -\omega & -\omega^2 \\ 1 & \omega^2 & \omega & -1 & -\omega^2 & -\omega \end{pmatrix}, \quad \omega = \exp(2\pi i/3) \qquad (2.10)$$

will diagonalize K_{dd}^{eff} as follows;

$$K_{dd}^{0}(E) =$$

$$\begin{pmatrix} \varepsilon_{dp}+6x(E)-E & & & & & \\ & \varepsilon_{dp}+3x(E)-E & & & & \\ & & \varepsilon_{dp}+3x(E)-E & & & \\ & & & \varepsilon_{dp}+2x(E)-E & & \\ & & & & \varepsilon_{dp}+5x(E)-E & \\ & & & & & \varepsilon_{dp}+5x(E)-E \end{pmatrix} . \qquad (2.11)$$

Setting the resulting diagonal elements equal to zero:

$$\varepsilon_{dp} + nx(E) - E = 0, \qquad n = 2,3,3,5,5,6 \qquad (2.12)$$

we obtain energy eigenvalues as

$$E(n) = \frac{1}{2(1-nS^2)} [\varepsilon_{dp} - 2n\gamma S + \sqrt{\varepsilon_{dp}^2 + 4n\gamma(\gamma - \varepsilon_{dp}S)}]. \qquad (2.13)$$

From Eq. (2.12) we also obtain another six solutions which are given by the expression similar to E(n) with negative sign in front of the square root. These energy eigenvalues correspond to six 3p band energies. Since we may assume $(\gamma/\varepsilon_{dp})^2 << 1$ and $S^2 << 1$, we have

$$E(n) = \varepsilon_{dp} + n\Gamma, \qquad \Gamma = \frac{\Gamma^2}{\varepsilon_{dp}} + \varepsilon_{dp}S^2 - 2\gamma S. \qquad (2.14)$$

γ is expected to be negative so that $\Gamma > 0$. Hence the singlet state for n=2 has the lowest energy, and two doublets for n=3 and n=5 and another singlet for n=6 have higher energies.

Eigenfunctions are obtained as follows. Corresponding to the transformation with A(E,k) of Eq. (2.5), one has d-p hybridized Bloch functions in the form

$$d_i + \sum_j p_j A(E,k)_{ji},$$

where d_i stands for one of the six d Bloch functions of Eq. (2.1), p_j for one of the 18 p Bloch functions of Eq. (2.2), and $A(E,k)_{ji}$ are the matrix elements of $-K_{pp}^{-1}K_{pd}$ in Eq. (2.5). One has following explicit expressions of the d-p hybridized Bloch functions:

$$
\begin{aligned}
\xi_I' &= N^{-1/2}[\xi_I - \lambda\cdot\tfrac{1}{2}(-e_{23}p_{2y} + e_{23}^*p_{3y} - e_{12}p_{4z} + e_{12}^*p_{5z})],\\
\eta_I' &= N^{-1/2}[\eta_I - \lambda\cdot\tfrac{1}{2}(e_{13}p_{1z} - e_{23}p_{2x} + e_{23}^*p_{3x} - e_{13}^*p_{6z})],\\
\zeta_I' &= N^{-1/2}[\zeta_I - \lambda\cdot\tfrac{1}{2}(e_{13}p_{1y} - e_{12}p_{4x} + e_{12}^*p_{5x} - e_{13}^*p_{6y})],\\
\xi_{II}' &= N^{-1/2}[\xi_{II} - \lambda\cdot\tfrac{1}{2}(e_{23}^*p_{1y} + e_{12}^*p_{3z} - e_{23}p_{4y} - e_{12}p_{6z})],\\
\eta_{II}' &= N^{-1/2}[\eta_{II} - \lambda\cdot\tfrac{1}{2}(e_{23}^*p_{1x} - e_{13}^*p_{2z} - e_{23}p_{4x} + e_{13}p_{5z})],\\
\zeta_{II}' &= N^{-1/2}[\zeta_{II} - \lambda\cdot\tfrac{1}{2}(e_{13}^*p_{2y} + e_{12}^*p_{3x} + e_{13}p_{5y} - e_{12}p_{6x})],
\end{aligned}
\tag{2.15}
$$

where $e_{ij}=\exp[ik\cdot(\tau_i-\tau_j)/3]$, $\lambda=-2(\gamma-ES)/E$, and $N= 1+\lambda^2-4\lambda S$. With the use of Eq. (2.12) one obtains the relation between λ and γ as

$$
\gamma = -\frac{1}{2}\frac{\lambda - 2S}{1 - (n/4)\lambda^2}\,\varepsilon_{dp} \approx -\frac{1}{2}(\lambda - 2S)\varepsilon_{dp}. \tag{2.16}
$$

Furthermore, using Eq. (2.16), one obtains for Γ of Eq. (2.14) a simple expression (to order λ^2):

$$
\Gamma = \frac{1}{4}\lambda^2\varepsilon_{dp}. \tag{2.17}
$$

The final Bloch functions can be written as follows:

$$\psi_{1-} = \frac{1}{\sqrt{6}} [(e_2^*\xi_I' + e_3^*\eta_I' + e_1^*\zeta_I') - (e_2\xi_{II}' + e_3\eta_{II}' + e_1\zeta_{II}')]$$

(the first singlet),

$$\psi_{2a+} = \frac{1}{\sqrt{6}} [(e_2^*\xi_I' + \omega e_3^*\eta_I' + \omega^2 e_1^*\zeta_I') + (e_2\xi_{II}' + \omega e_3\eta_{II}' + \omega^2 e_1\zeta_{II}')]$$

ψ_{2b+} = similar expression with ω and ω^2 interchanged

(the first doublet),

ψ_{2a-} and ψ_{2b-} = similar to the above with - in the middle

(the second doublet),

ψ_{1+} = similar to ψ_{1-} with + in the middle

(the second singlet). (2.18)

Considering a Ti^{3+} site and the surrounding six Cl^- sites, we will see that the coefficients e_{ij} in the functions Eq. (2.15) just cancel the phases of the respective p Bloch functions at the Cl^- sites relative to the phase of the d Bloch function at the central Ti^{3+} site, since $(\tau_i - \tau_j)/3$ are the vectors joining the six Cl^- sites to the central Ti^{3+} site. Hence, the Bloch functions Eq. (2.15) can be constructed from d-p hybridized molecular orbitals or LCAO's of the form

$$\xi_I'' = \xi_I - \frac{\lambda}{2}(-p_{2y} + p_{3y} - p_{4z} + p_{5z}), \quad \text{etc.}, \tag{2.19}$$

where λ depends slightly on n as seen by Eq. (2.16). However,

n dependence of λ can be safely neglected. In fact, the Wannier functions constructed from each band are linear combinations of the molecular orbitals Eq. (2.19) and have forms similar to Eq. (2.18):

$$\begin{aligned}
&(\xi''_{I} + \eta''_{I} + \zeta''_{I}) \mp (\xi''_{II} + \eta''_{II} + \zeta''_{II}), \\
&(\xi''_{I} + \omega\eta''_{I} + \omega^2\zeta''_{I}) \mp (\xi''_{II} + \omega\eta''_{II} + \omega^2\zeta''_{II}), \\
&(\xi''_{I} + \omega^2\eta''_{I} + \omega\zeta''_{I}) \mp (\xi''_{II} + \omega^2\eta''_{II} + \omega\zeta''_{II}).
\end{aligned} \tag{2.20}$$

Here ξ''_{I}, η''_{I}, ζ''_{I}, $-\xi''_{II}$, $-\eta''_{II}$, $-\zeta''_{II}$, for example for the first function, are associated with the six corners of each hexagon of the honeycomb lattice in the way shown in Fig. 2-4 with letters written outside each hexagon. Neighboring Wannier functions are orthogonal for the reason that there is no p orbital shared by two Wannier functions. Since we have assumed no transfer between orthogonal atomic orbitals, there is also no transfer between Wannier functions. The zero width of all the bands results in this way.

2.2 Numerical calculation

We estimate the parameters ε_{dp}, λ, and S. The Madelung potential energy was calculated for the Ti^{3+} site and for the Cl^- site, and we obtained 1.129 Ryd. (by the Evjen method) and -0.790 Ryd. (by the Ewald method), respectively. Experimental values of the ionization energy of the free Ti^{3+} and the electron affinity of the free Cl atom are 1.958 Ryd. and 0.237 Ryd., respectively. Hence

$$\varepsilon_d = 1.129 - 1.958 = -0.829, \quad \varepsilon_p = -0.790 - 0.237 = -1.027,$$

$$\varepsilon_{dp} = \varepsilon_d - \varepsilon_p = 0.198 \text{ Ryd.}$$

This is a rough estimate for several reasons. If we take a calculated value[5] of 2.046 Ryd. for the ionization energy of Ti^{3+}, then we have $\varepsilon_{dp} = 0.110$ Ryd.. We have neglected electronic polarizations of the Cl^- ions in the crystal of $TiCl_3$. The ionization energy and the electron affinity may take slightly different values in the crystal. Also, the charge distribution resulting from partial covalent bonding and antibonding between Ti and Cl, i.e., the charge distribution to result from our band model, would be slightly different from that of the purely ionic crystal.

We have calculated S using the Slater functions for Ti^{3+} and Cl^- as a function of their distance (see Fig. 2-5). For the observed distance, 2.45 Å, we obtained S=0.14, which may be an

overestimated value because of the nature of the Slater functions. λ should exceed 2S as γ should be negative, and we assume values of λ around 3S. For S=0.1 and λ=3S the energy separation Γ given by Eq. (2.17) is estimated to be 0.0605 eV=704 K. In Fig. 2-6 for various values of S and λ we show the band energies calculated with the use of Eq. (2.13).

Figure Captions

Fig. 2-1. The crystal structure of α (a) and γ (b) modifications of $TiCl_3$.

Fig. 2-2. A sandwich layer of $TiCl_3$.

Fig. 2-3. Indirect d-d hybridization through a 3p orbital.

Fig. 2-4. The Wannier function for the lowest singlet band.

Fig. 2-5. Plot of the overlap integral S vs. the Ti-Cl distance ρ.

Fig. 2-6. S and λ dependence of the dε band energies.

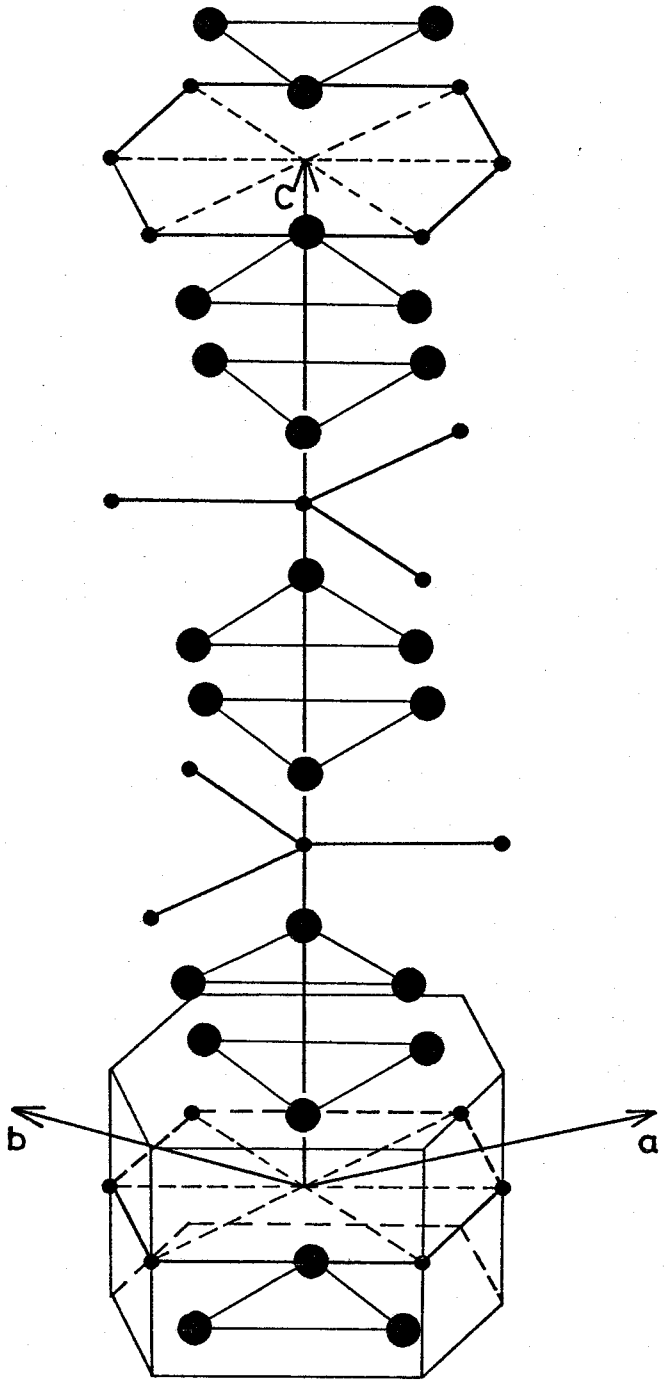

$\alpha - TiCl_3$

Fig. 2-1a

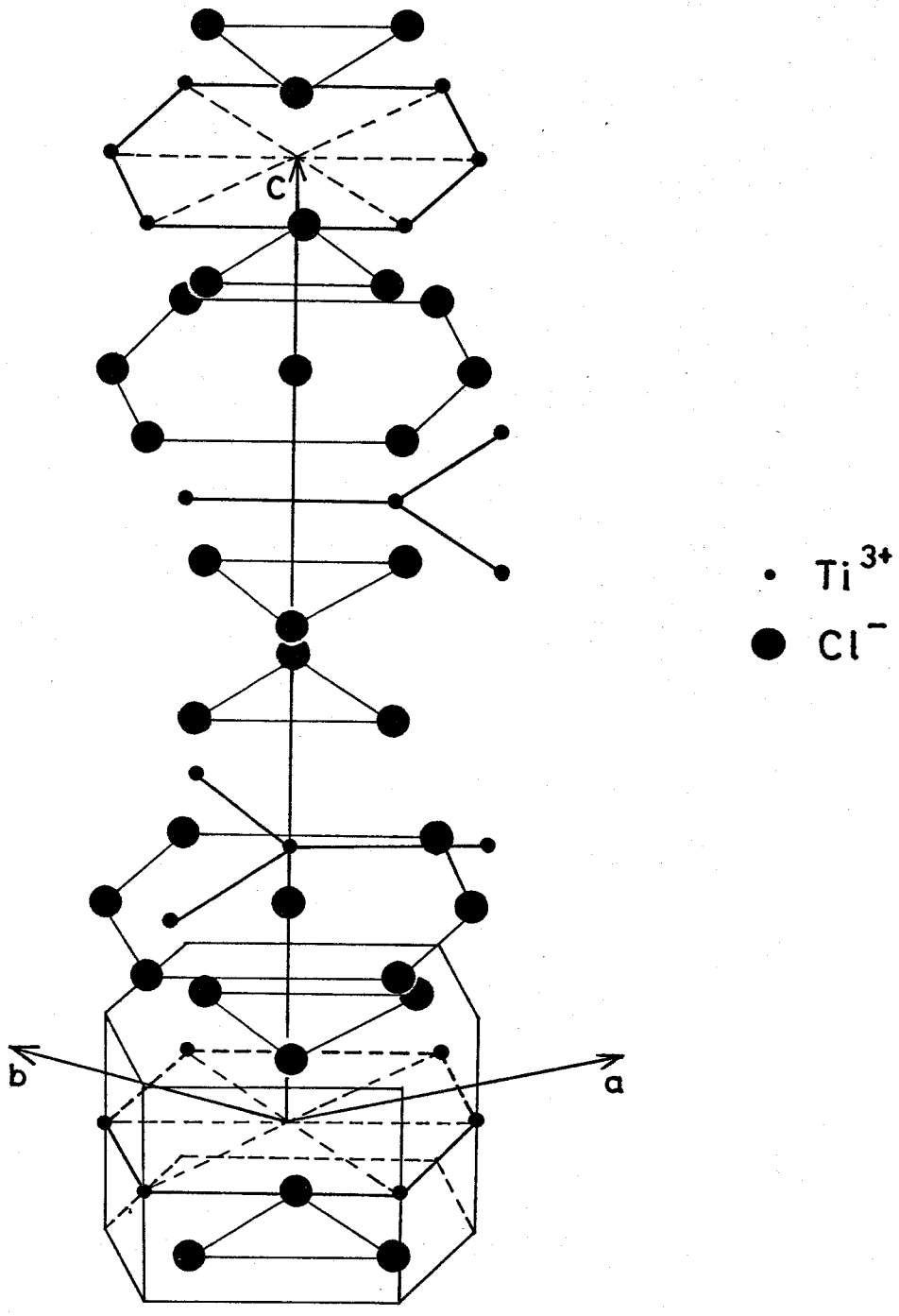

γ−TiCl$_3$

Fig. 2-1b

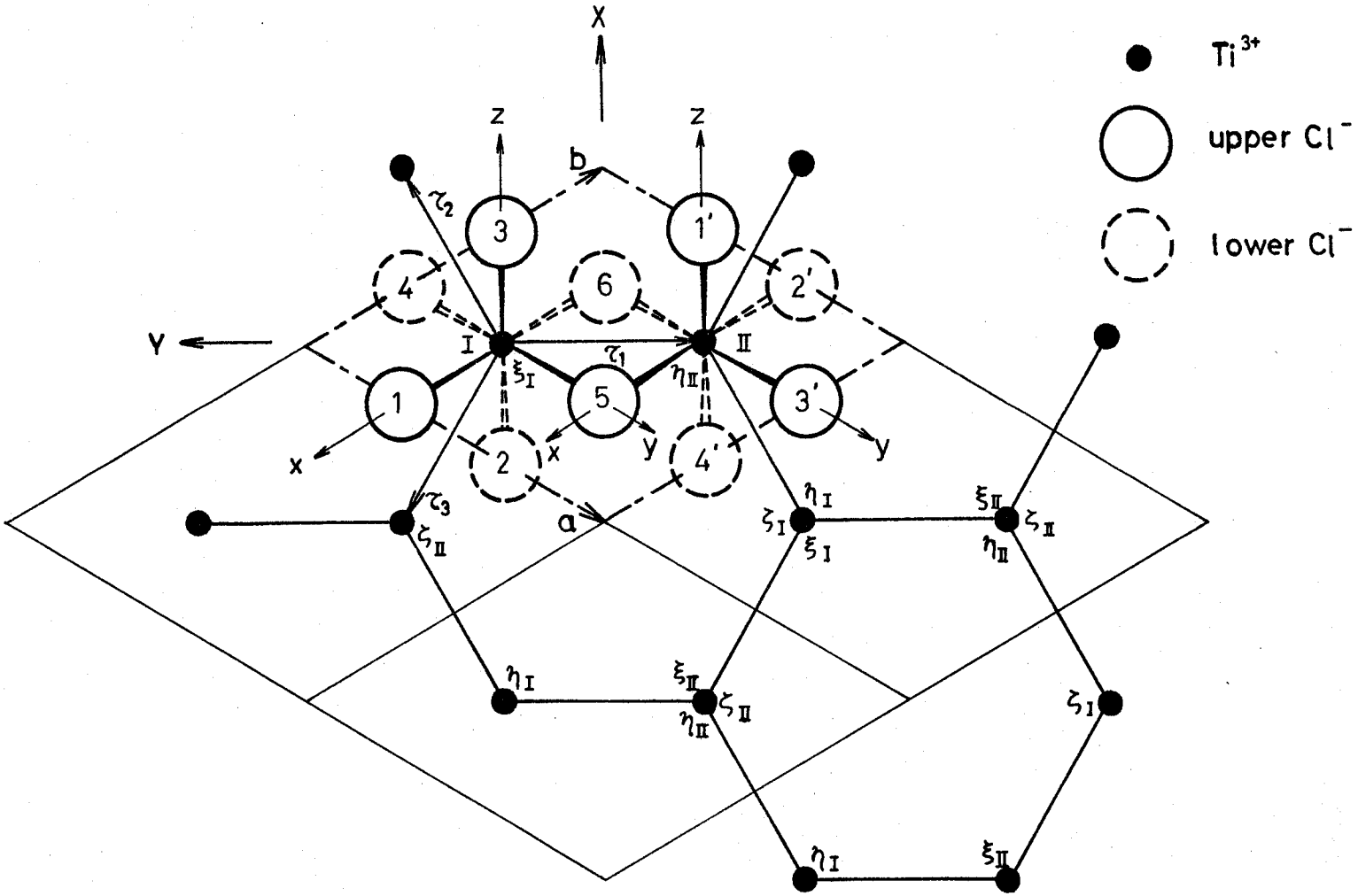
X
Z
Z
b
Y
I
II
1
2
3
4
5
6
1'
2'
3'
4'
x
y
x
y
a
τ_1
τ_2
τ_3
ξ_I
η_{II}
η_I
ζ_I
ξ_{II}
ζ_{II}
Ti^{3+}
upper Cl^-
lower Cl^-

Fig. 2-2

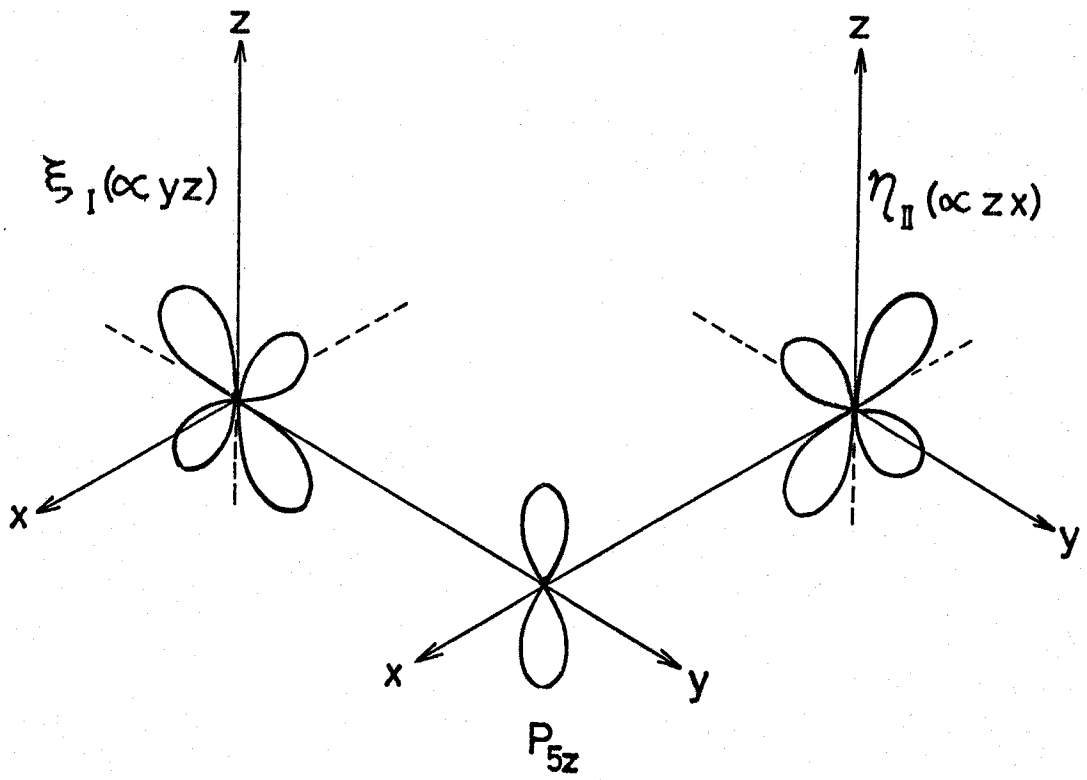

Fig.2-3

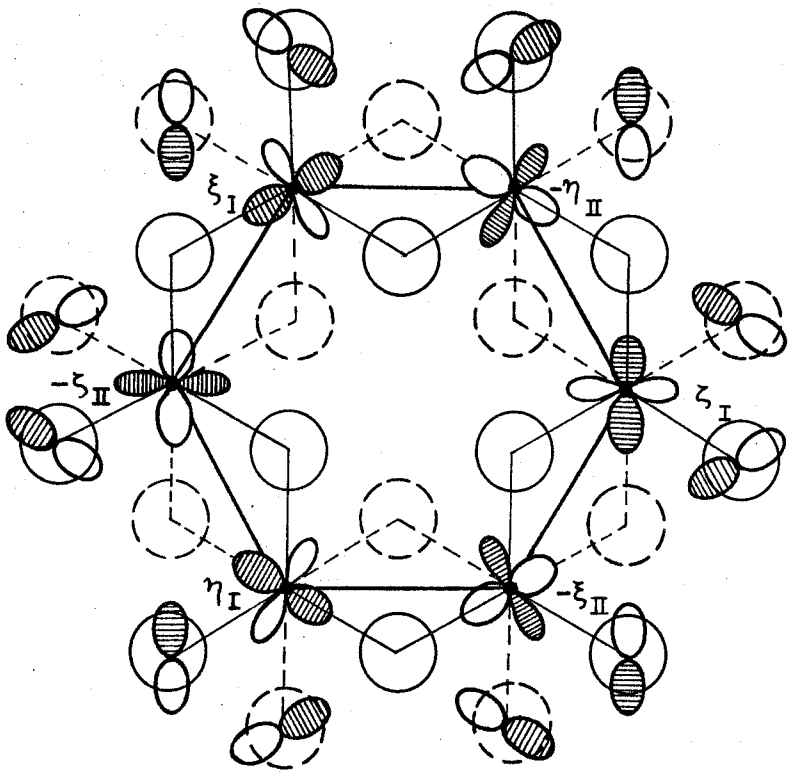

Fig.2-4

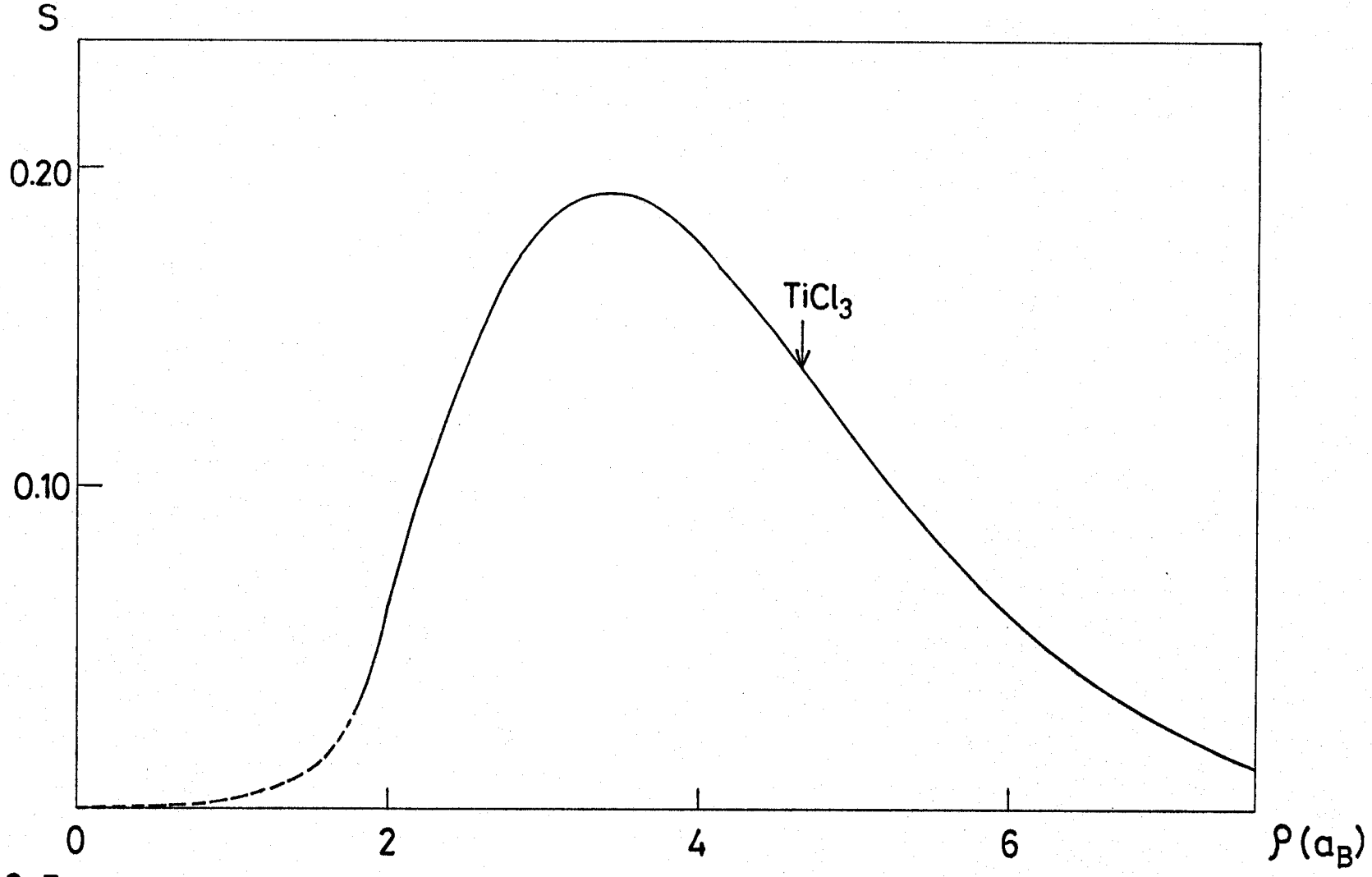

Fig.2-5

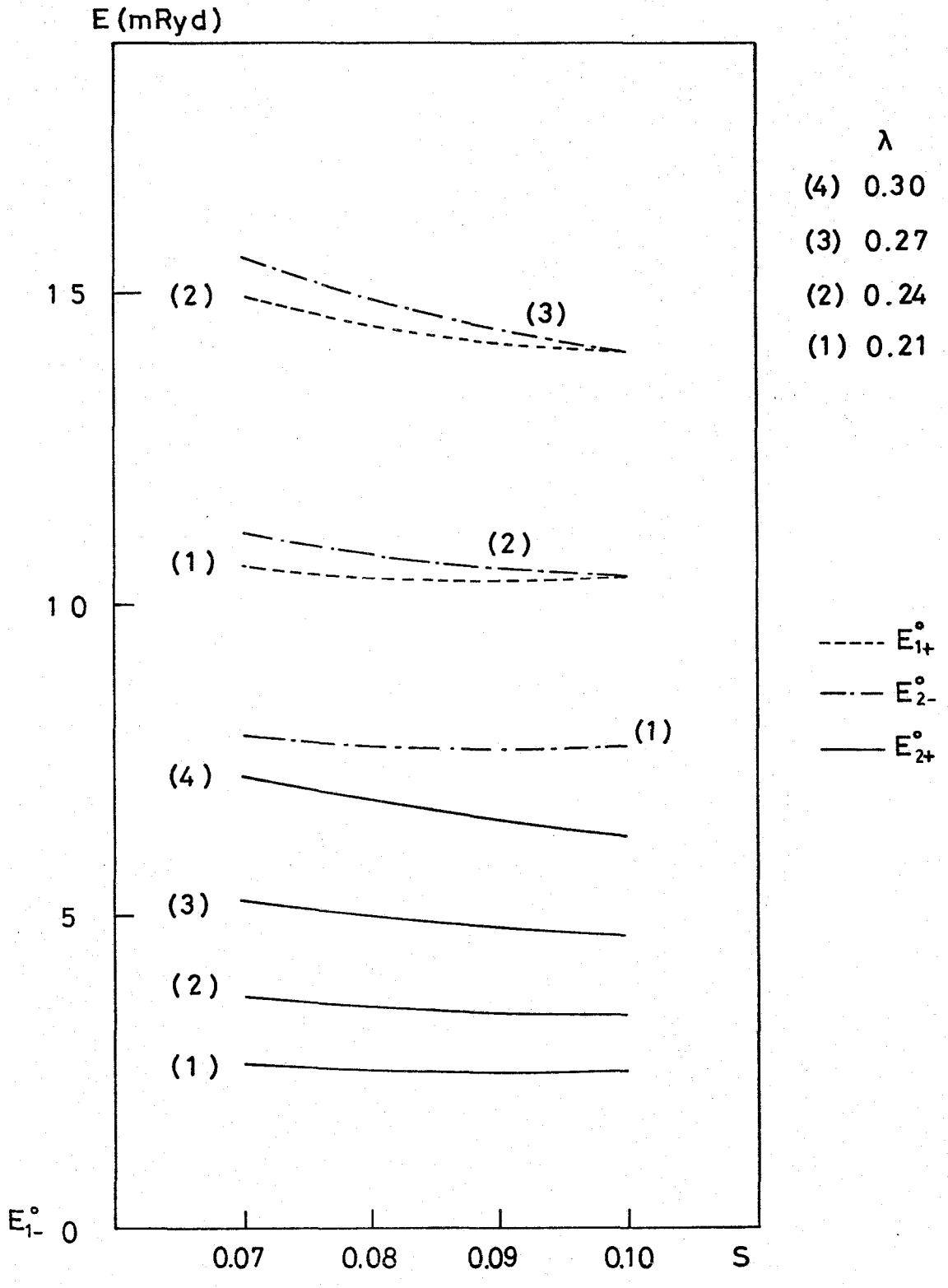
E (mRyd)
15
10
5
0
E°_{1-}
0.07
0.08
0.09
0.10
S
(1)
(2)
(3)
(4)
λ
(4) 0.30
(3) 0.27
(2) 0.24
(1) 0.21
E°_{1+}
E°_{2-}
E°_{2+}

Fig. 2-6

§3. Electronic Band Structure in Distorted Lattice

3.1 Formulation

As mentioned before, in the high temperature phase of the $TiCl_3$ crystal the Ti^{3+} ions form honeycomb lattices which intervene into the close-packed structure of the Cl^- ions. Each Ti^{3+} is surrounded by six Cl^- ions in octahedral configuration as shown in Fig. 2-2. The unit cell contains two Ti^{3+} ions (I and II) and six Cl^- ions (1,2,...,6). In the previous section we calculated the $d\varepsilon$ bands in the high temperature structure and obtained dispersionless singlet and doublet bands. We now calculate the band energies in a distorted lattice. Here we consider three types of distortion of the Ti^{3+} lattice, denoted as antidimerization, dimerization, and shear, which are shown in Fig. 3-1.

In the previous calculation of the energy bands in the high temperature structure two parameters γ and S were used, the transfer and overlap integrals, respectively, between nonorthogonal atomic orbitals of a Ti^{3+} and its nearest neighboring Cl^-. In a distorted structure we must consider changes in S and γ and additional overlap and transfer integrals between those atomic orbitals which have become nonorthogonal due to distortion. We calculate these quantities to first order in Ti^{3+} displacement δr. For the change of S and the new overlap integrals we have

$$\int \phi_p \phi_{d\varepsilon} d\tau - \int \phi_p (\phi_{d\varepsilon})_0 = \int \phi_p (\mathrm{grad}\phi_{d\varepsilon})_0 d\tau \cdot \delta\vec{r}, \qquad (3.1)$$

where suffix 0 means the value at the position in the undistorted lattice. For the integral in the right-hand side of Eq. (3.1) we have three different integrals, S', S'_σ, and S'_π. For example, for Ti^{3+} at site I and Cl^- at site 5 (see Fig. 2-2), these are

$$\begin{aligned} S' &\equiv \int p_{5x}(\partial\zeta_I/\partial y)_0 d\tau = \int p_{5z}(\partial\xi_I/\partial y)_0 d\tau, \\ S'_\sigma &\equiv \int p_{5y}(\partial\zeta_I/\partial x)_0 d\tau = \int p_{5y}(\partial\xi_I/\partial z)_0 d\tau, \\ S'_\pi &\equiv -\int p_{5x}(\partial\eta_I/\partial z)_0 d\tau = -\int p_{5z}(\partial\eta_I/\partial x)_0 d\tau, \end{aligned} \tag{3.2}$$

where $\xi_I(\propto yz)$ etc. are the $d\varepsilon$ atomic wave functions at site I and $p_{5x}(\propto x)$ etc. the p atomic wave functions at site 5, x, y, and z representing local cubic axes shown in Fig. 2-2. The arrangements of the wave functions are illustrated in Fig. 3-2. Thus, for small displacement δr, S changes to $S+S'\delta r$ and two additional overlap integrals, $S'_\sigma\delta r$ and $S'_\pi\delta r$, are introduced. Similarly, the transfer integral γ changes to $\gamma+\gamma'\delta r$ and two additional transfer integrals, $\gamma'_\sigma\delta r$ and $\gamma'_\pi\delta r$, are considered.

As in §2, we calculate the band energy in the tight-binding approximation. Using 24 Bloch functions we construct energy matrix H(k) and overlap matrix S(k). The band energy E is obtained from the equation

$$\det|K(E,k)| \equiv \det|H(k) - ES(k)| = 0. \tag{3.3}$$

We can write

$$K(E,k) = \begin{bmatrix} K_{dd} & K_{dp} \\ K_{pd} & K_{pp} \end{bmatrix}, \tag{3.4}$$

where

$$K_{dd} = (\varepsilon_d - E)\ I_6, \text{ and } K_{pp} = (\varepsilon_p - E) I_{18}.$$

I_6 and I_{18} are unit matrices of dimension 6 and dimension 18, respectively, and ε_d and ε_p the energies of the 3dε and 3p levels in the crystal. We write $\varepsilon_{dp}=\varepsilon_d-\varepsilon_p$ and set $\varepsilon_p=0$. K_{pd} is the sum of $K_{pd}^{(0)}$ of the undistorted lattice and ΔK_{pd} which is linear in the displacement. The matrix element of $K_{pd}^{(0)}+K_{pd}$ is shown in Appendix 1. The effective matrix $K_{dd}^{eff}(E,k)$ defined by Eq. (2.7) now changes to first order in δr by

$$\Delta K_{dd}^{eff} = -[K_{dp}^{(0)}\ K_{pp}^{-1}\ \Delta K_{pd} + (h.c.)]. \tag{3.5}$$

Solving $\det|K_{dd}^{eff}(E,k)|=0$ with the use of the same transformations as those used in §2, we obtain band energies E(k) as functions of the displacement. The energy eigenvalues are obtained in the following form:

the first singlet:

$$E_{1-}(k) = E_{1-}^{(0)} + \frac{\gamma - E_{1-}^{(0)}S}{\sqrt{(\varepsilon_{dp})^2 + 8\gamma(\gamma - S\varepsilon_{dp})}} M_-,$$

the first doublet:

$$E_{2+}(k) = E_{2+}^{(0)} + \frac{\gamma - E_{2+}^{(0)}S}{\sqrt{(\varepsilon_{dp})^2 + 12\gamma(\gamma - S\varepsilon_{dp})}} [M_+^{aa} \mp |M_+^{ab}|],$$

(3.6)

the second doublet:

$$E_{2-}(k) = E_{2-}^{(0)} + \frac{\gamma - E_{2-}^{(0)}S}{\sqrt{(\varepsilon_{dp})^2 + 20\gamma(\gamma - S\varepsilon_{dp})}} [M_-^{aa} \mp |M_-^{ab}|],$$

the second singlet:

$$E_{1+}(k) = E_{1+}^{(0)} + \frac{\gamma - E_{1+}^{(0)}S}{\sqrt{(\varepsilon_{dp})^2 + 24\gamma(\gamma - S\varepsilon_{dp})}} M_+,$$

where $M_\pm$, $M_\pm^{aa}$, and $M_\pm^{ab}$ are linear in the displacement δr and are functions of wavevector k as shown in Appendix 2; Each band has a dispersion. The band energies in the undistorted lattice are denoted by the superscript (0) and are given by Eq. (2.13). In Eq. (3.6) we neglected the quadratic term in δr and considered only the intraband mixing due to the lattice distortion.

3.2 Numerical results

The additional parameters involved are estimated as follows: S', S'_σ and S'_π are calculated using the Slater functions for 3dε orbitals of Ti^{3+} and for 3p's of Cl^-. We obtain $S':S'_\sigma:S'_\pi = 1:2.91:0.30$ for the observed Ti-Cl distance ρ_0=2.45 A in the undistorted lattice. We set, as an example $S'=0.0655$ (a.u.)$^{-1}$. The ratios of γ'_σ and γ'_π to γ' are assumed to be similar to those of S'_σ and S'_π to S'. Further, a relation $\gamma'/\gamma = \alpha S'/S$ is assumed, α being an ajustable parameter that varies between 1/2 and 2. As discussed in §2, γ is related to the covalency parameter λ through Eq. (2.16), and ε_{dp} was estimated to be 0.198 Ryd.. Hence in our calculations S, λ and α remain disposable parameters.

In Fig. 3-3 we show the calculated dispersion curves for the lowest singlet band and the lower doublet band in the antidimerization, dimerization, and shear structures. The values of $\delta r/\tau$ used in these calculations correspond to the respective equilibrium displacement at 0 K, which will be determined self-consistently as shown later. We have calculated the density of states of the first singlet band and the first doublet band as functions of δr, for the antidimerization, the dimerization, and the shear, respectively. For small displacement a gap exists between the singlet band and the doublet band. If the magnitude of the displacement exceeds some critical value δr_c, the lower branch of the doublet band overlaps with the lowest singlet band. Such behavior is shown in Fig. 3-4. The obtained values of $\delta r_c/\tau$ are 0.84, 0.75, and 0.67% for the antidimerization, the dimerization, and the shear

respectively. For $\delta r > \delta r_c$ the Fermi level in the distorted structure lowers as shown in Fig. 3-5 and the electronic energy decreases proportional to $\delta r - \delta r_c$. On the other hand there is an increase of the lattice energy due to interatomic forces which is proportional to $(\delta r)^2$. An equilibrium displacement at 0 K is determined from the balance of these two energies.

Figure Captions

Fig. 3-1. Three kinds of lattice distortion. Two Ti ions in the unit cell shown by the dotted line move against each other.

Fig. 3-2. Additional overlap integrals. When the Ti ion is displaced in the direction shown by the arrow, each integral takes a positive value.

Fig. 3-3. The dispersion curves for the $d\varepsilon$ band in the antidimerized (a), dimerized (b), and sheared (c) structures. Assumed magnitude of the displacement is the equilibrium value in the distorted structure at 0 K.

Fig. 3-4. The density of states of low lying three bands for $\delta r/\tau$ = 0.75%. The lower two bands are separated by a small gap for the antidimerization (a), are just touched for the dimerization (b), and overlap each other for the shear (c).

Fig. 3-5. The $d\varepsilon$ band structure for the antidimerized (a), the dimerized (b), and the sheared (c) lattices in their equilibrium states at 0 K. The whole structure is almost symmetric about its center.

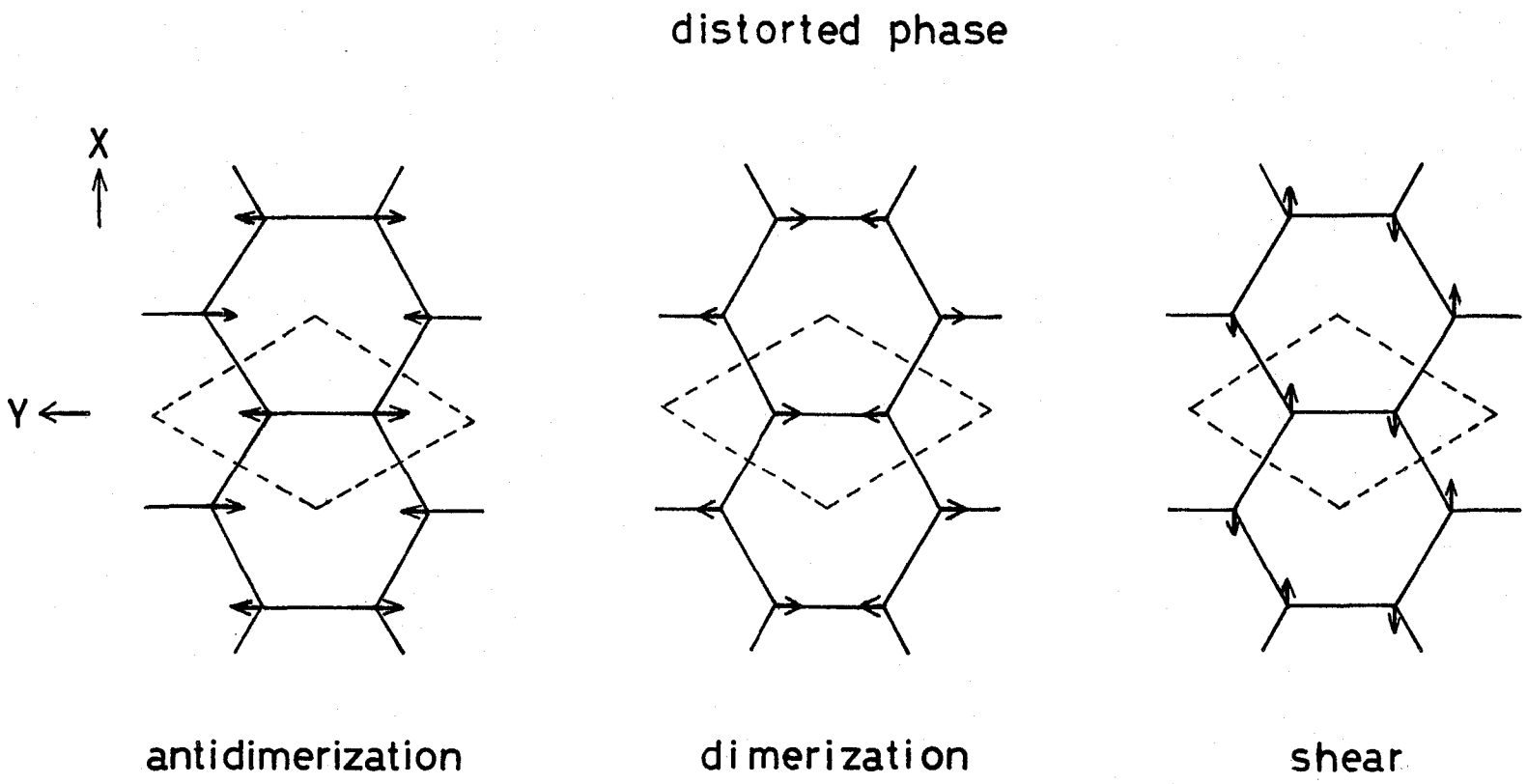

Fig. 3-1

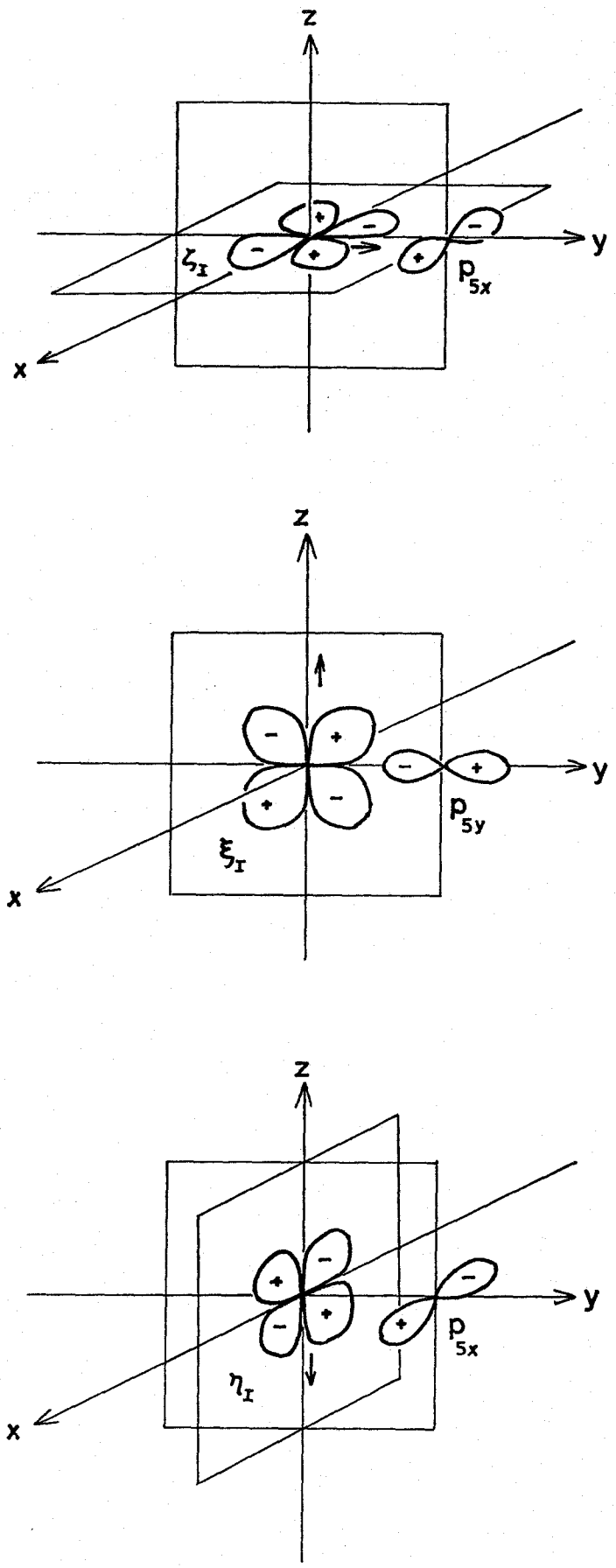

Fig.3-2

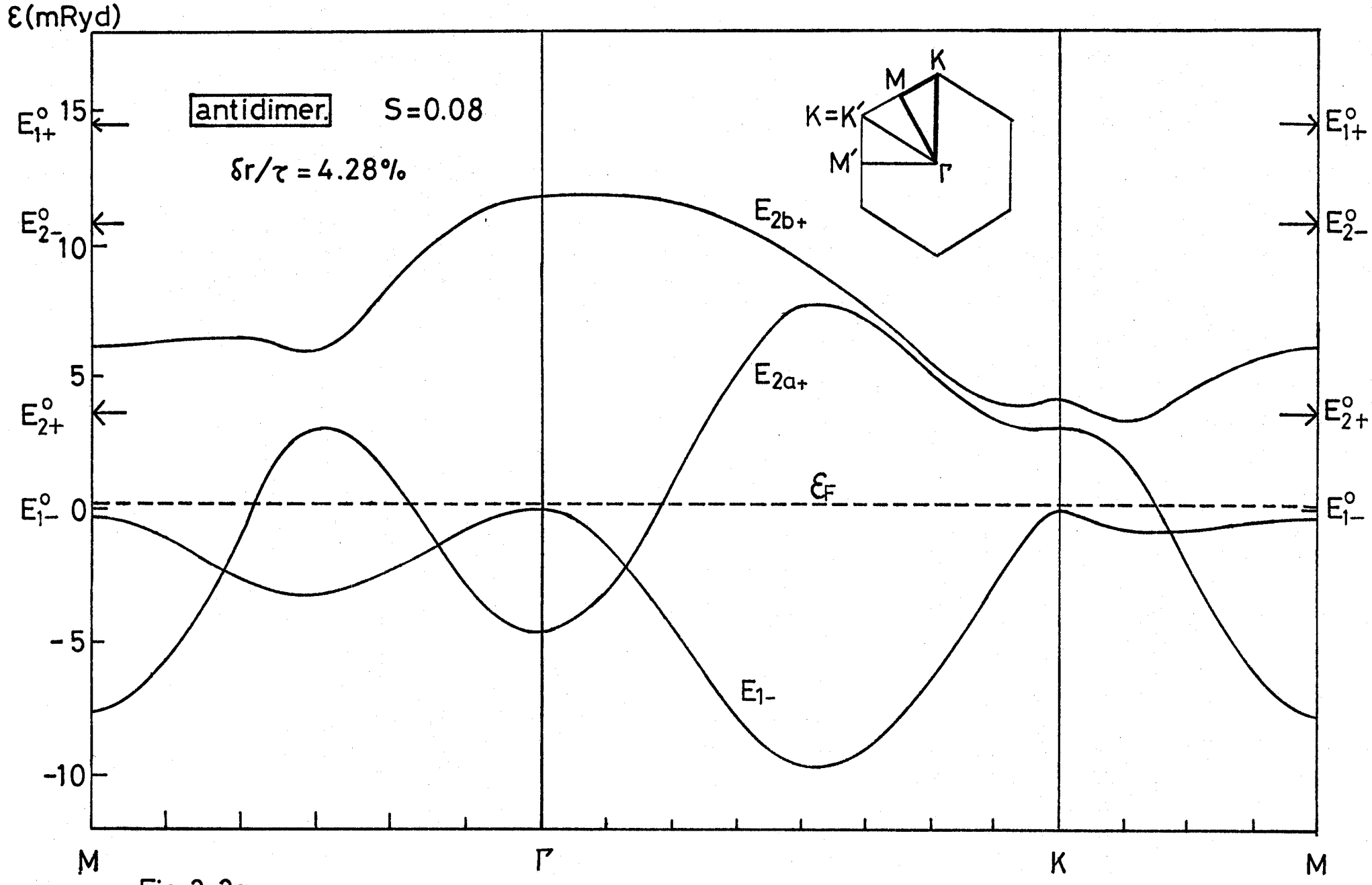
ε(mRyd)
antidimer.
S=0.08
δr/τ = 4.28%
K
M
K=K'
M'
Γ
E2b+
E2a+
E1-
εF
E°1+ 15
E°2- 10
5
E°2+
E°1- 0
-5
-10
E°1+
E°2-
E°2+
E°1-
M
Γ
K
M

Fig.3-3a

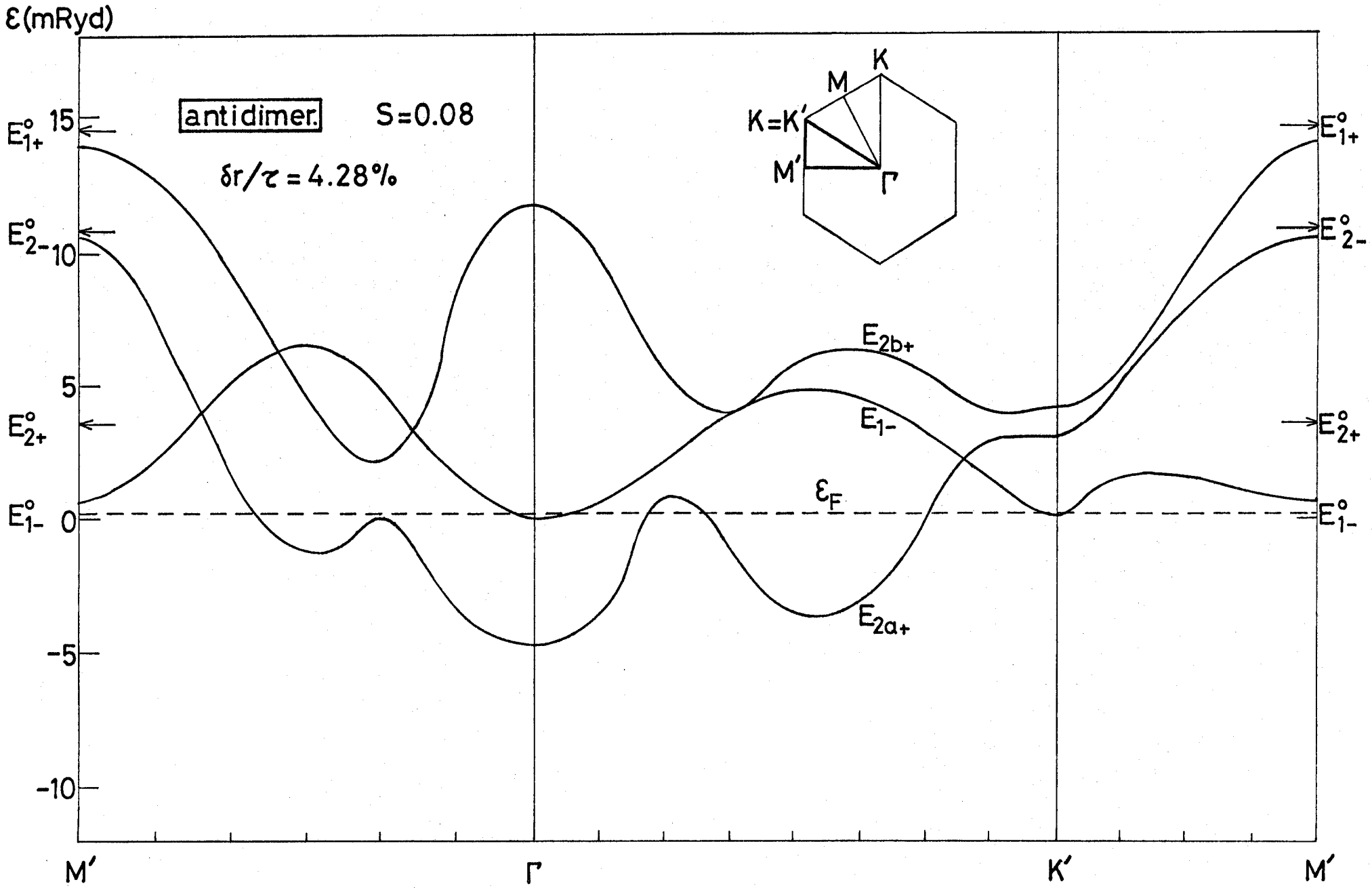
ε(mRyd)
antidimer.
S=0.08
δr/τ = 4.28%
K
M
K=K'
M'
Γ
E°1+
E°2-
E°2+
E°1-
15
10
5
0
-5
-10
E2b+
E1-
εF
E2a+
M'
Γ
K'
M'

Fig.3-3a

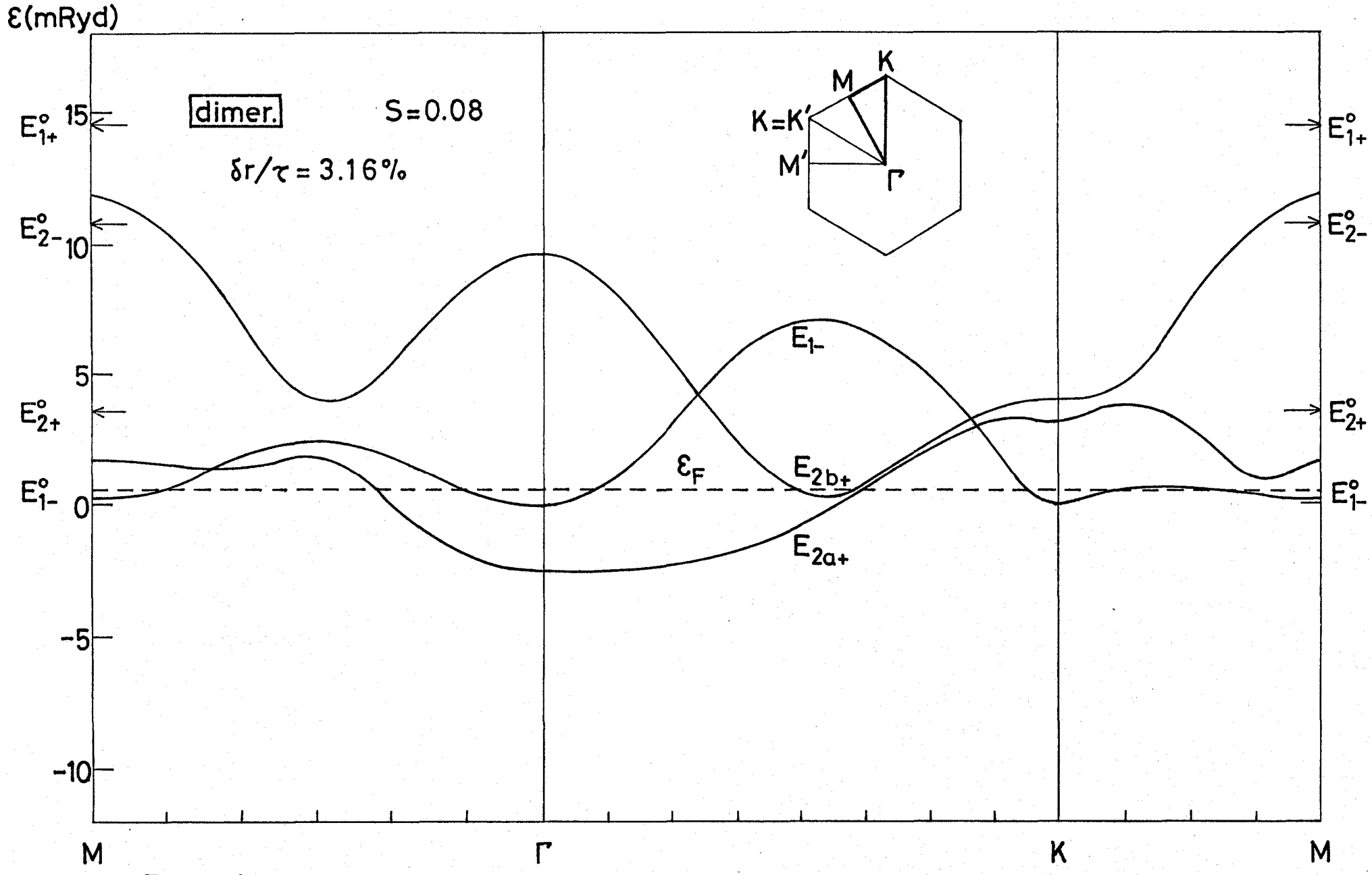
ε(mRyd)
dimer.
S=0.08
δr/τ = 3.16%
K
M
K=K'
M'
Γ
E°1+
E°2-
E°2+
E°1-
15
10
5
0
-5
-10
E1-
E2b+
E2a+
εF
M
Γ
K
M

Fig.3-3b

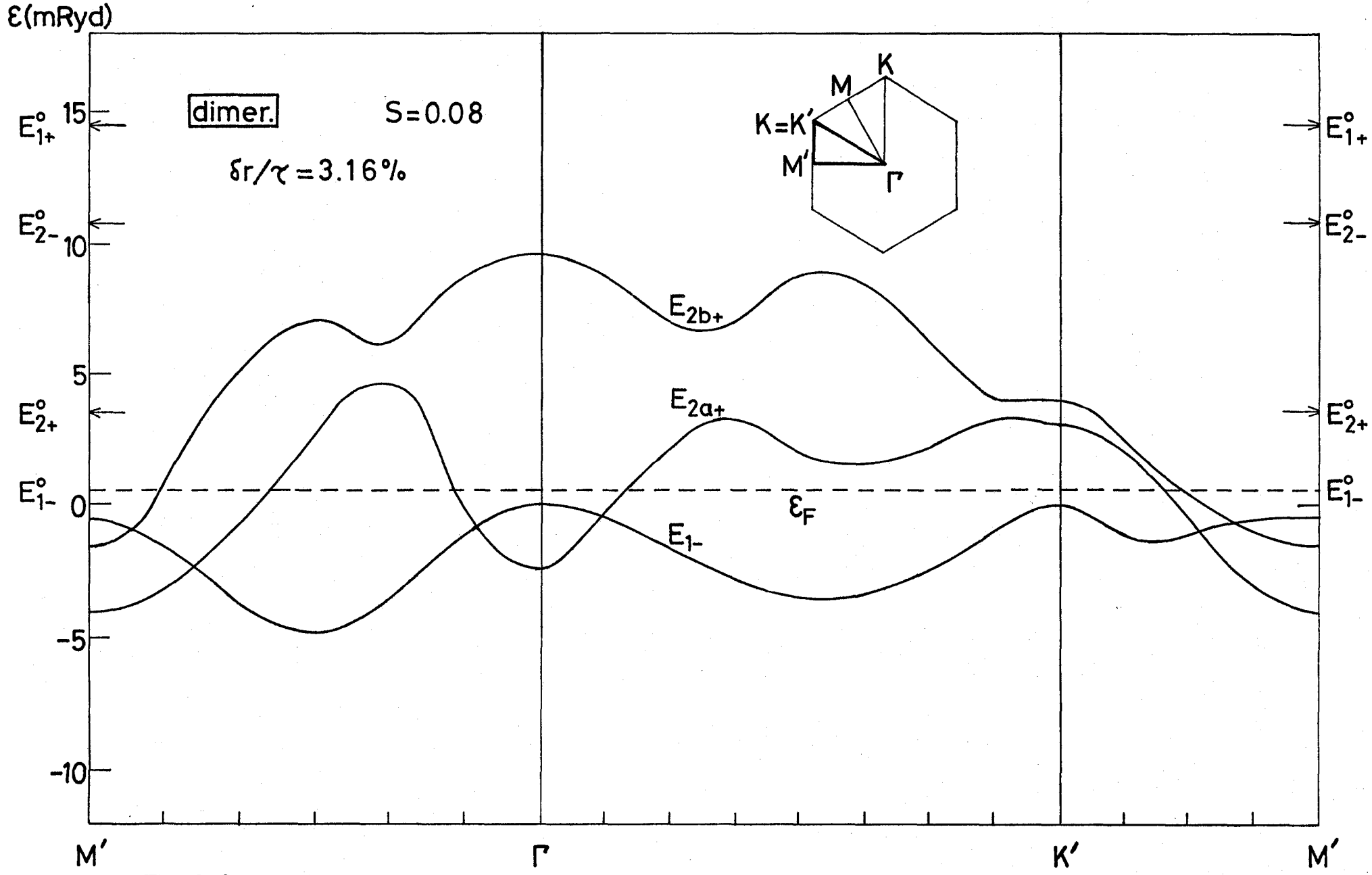
ε(mRyd)
dimer.
S=0.08
δr/τ=3.16%
K
M
K=K'
M'
Γ
E°1+
E°2-
E°2+
E°1-
15
10
5
0
-5
-10
E2b+
E2a+
E1-
εF
M'
Γ
K'
M'

Fig.3-3b

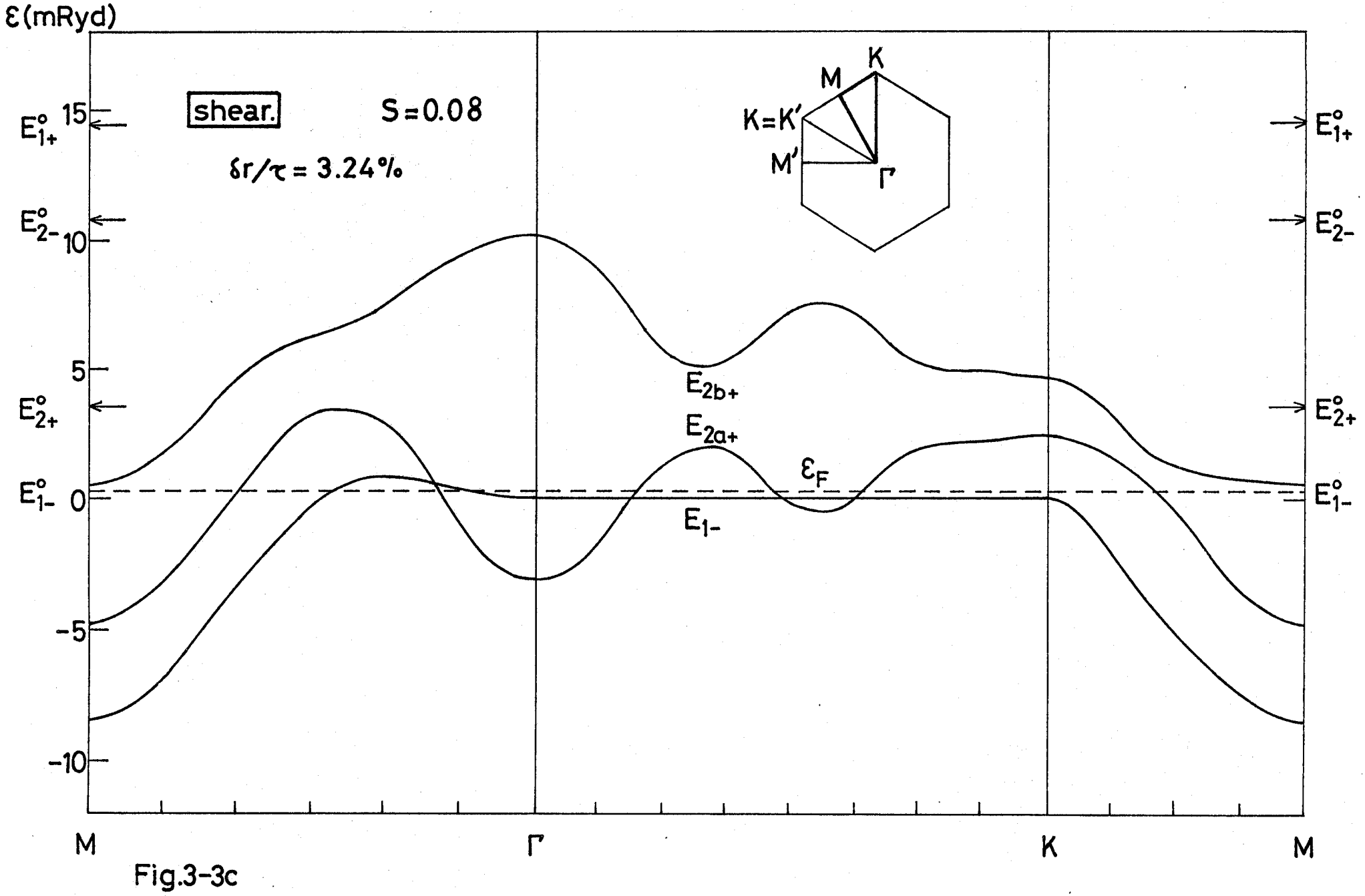
ε(mRyd)
shear.
S=0.08
δr/τ = 3.24%
K
M
K=K'
M'
Γ
15
10
5
0
-5
-10
E°_{1+}
E°_{2-}
E°_{2+}
E°_{1-}
E_{2b+}
E_{2a+}
ε_F
E_{1-}
M
Γ
K
M

Fig.3-3c

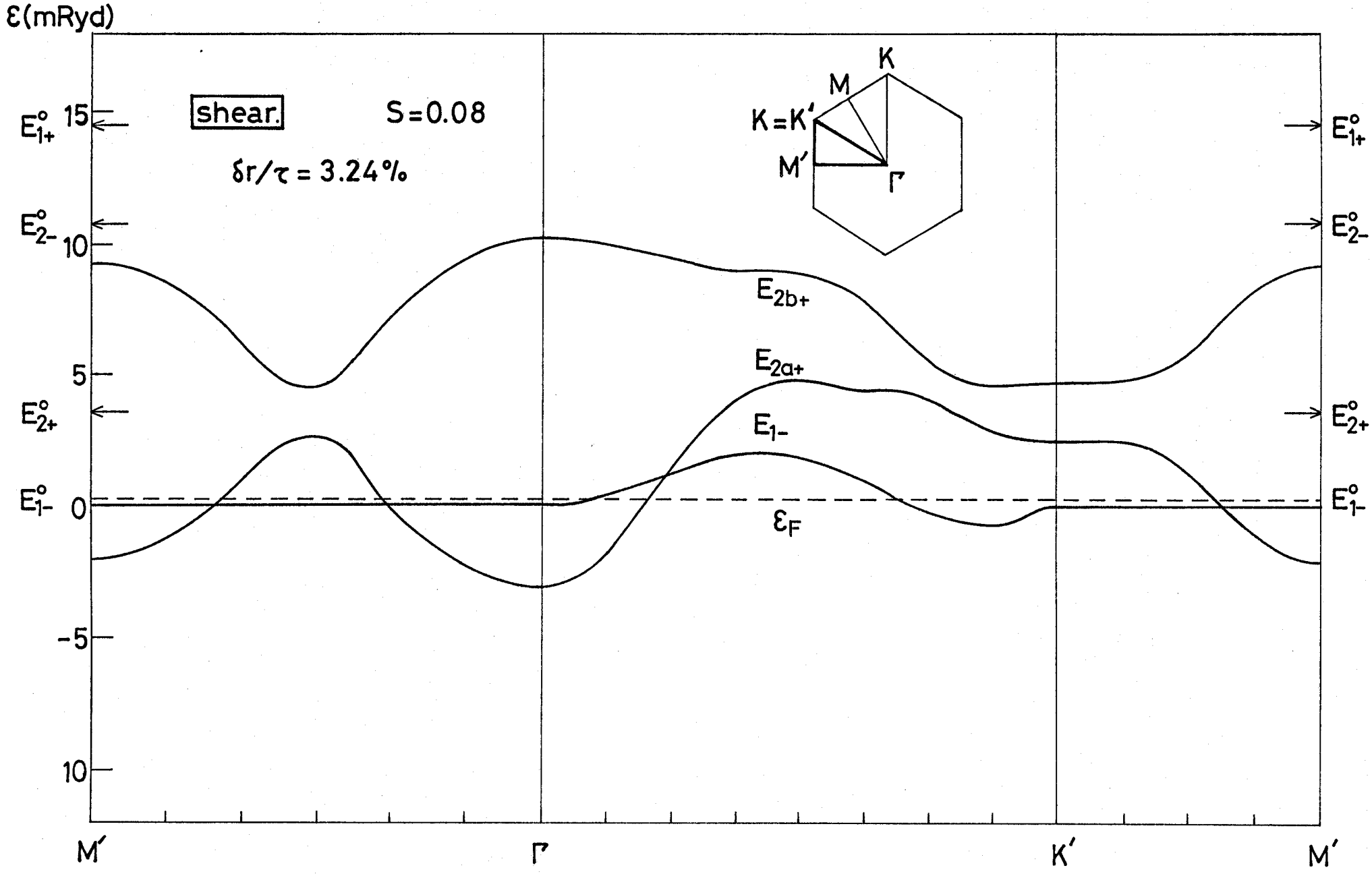
ε(mRyd)
shear.
S=0.08
δr/τ = 3.24%
K
M
K=K'
M'
Γ
E°1+
E°2-
E°2+
E°1-
15
10
5
0
-5
10
E2b+
E2a+
E1-
εF
M'
Γ
K'
M'

Fig.3-3c

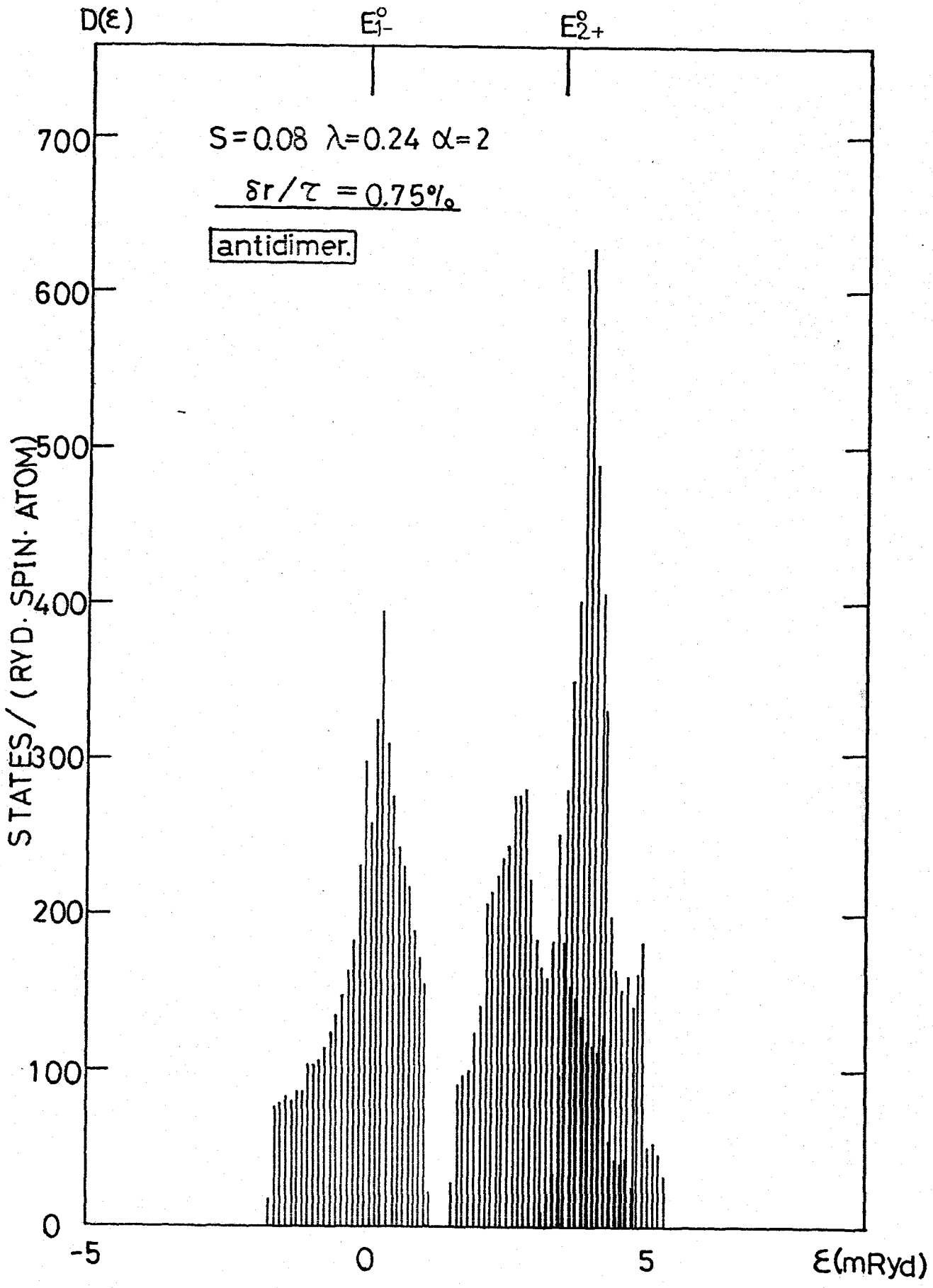
D(ε)
E1°-
E2°+
S=0.08 λ=0.24 α=2
δr/τ =0.75%
antidimer.
700
600
500
400
300
200
100
0
STATES/(RYD. SPIN. ATOM)
-5
0
5
ε(mRyd)

Fig.3-4a

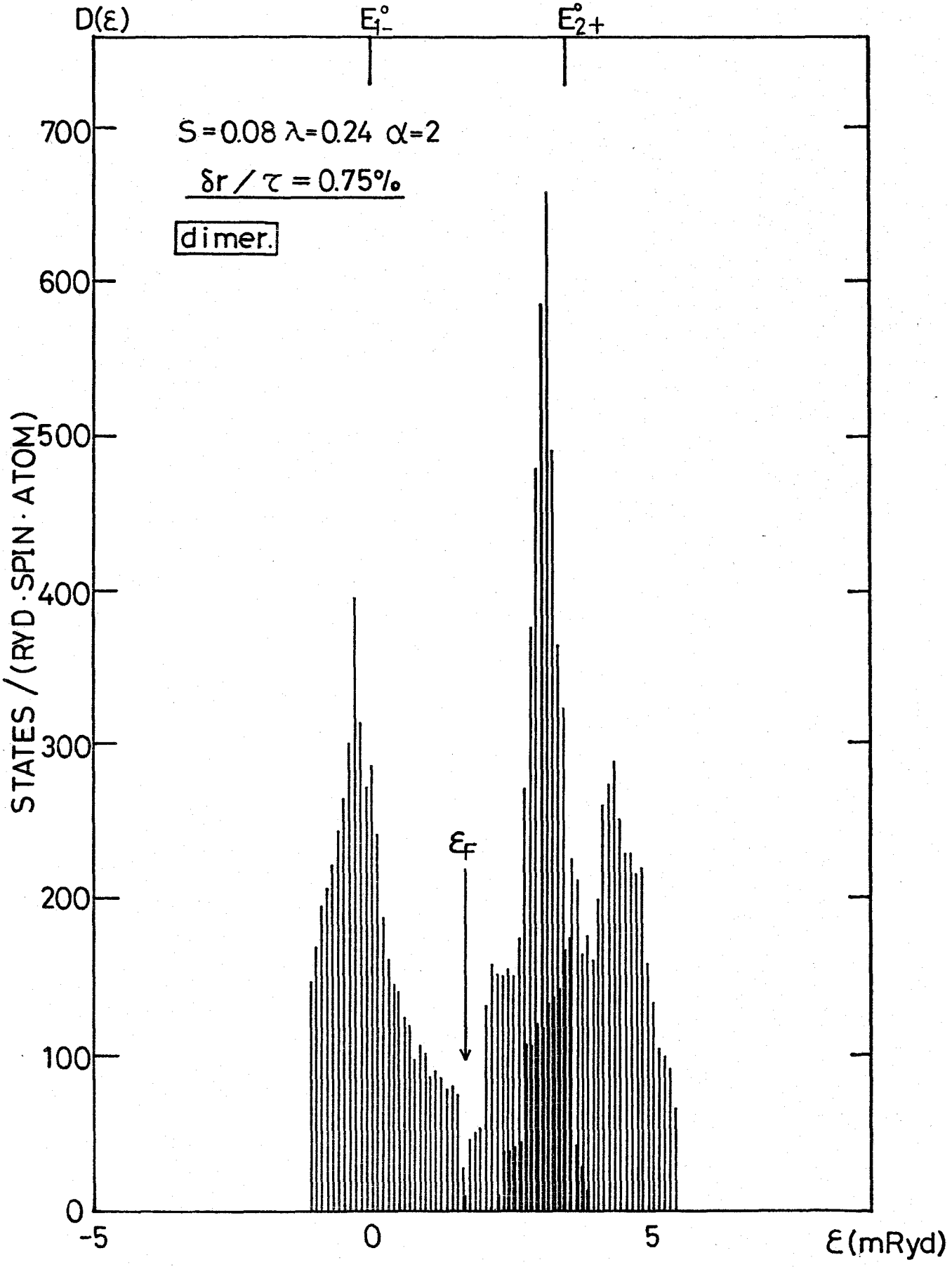
D(ε)
E1-°
E2+°
S=0.08 λ=0.24 α=2
δr/τ=0.75%
dimer.
700
600
500
400
300
200
100
0
STATES /(RYD·SPIN·ATOM)
εF
-5
0
5
ε(mRyd)

Fig. 3-4b

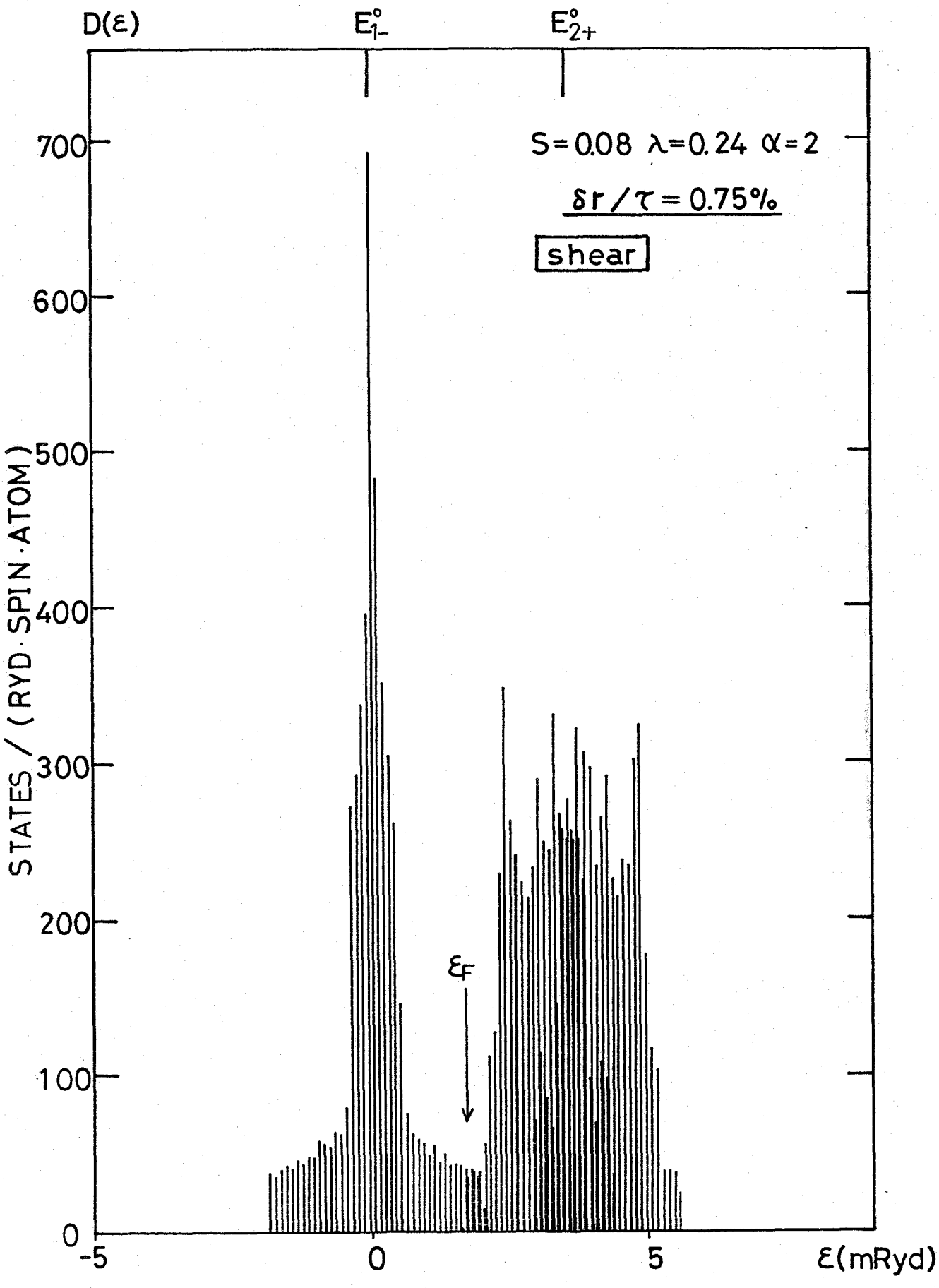
D(ε)
E°1-
E°2+
S=0.08 λ=0.24 α=2
δr/τ=0.75%
shear
700
600
500
400
300
200
100
0
STATES / (RYD·SPIN·ATOM)
εF
-5
0
5
ε(mRyd)

Fig.3-4c

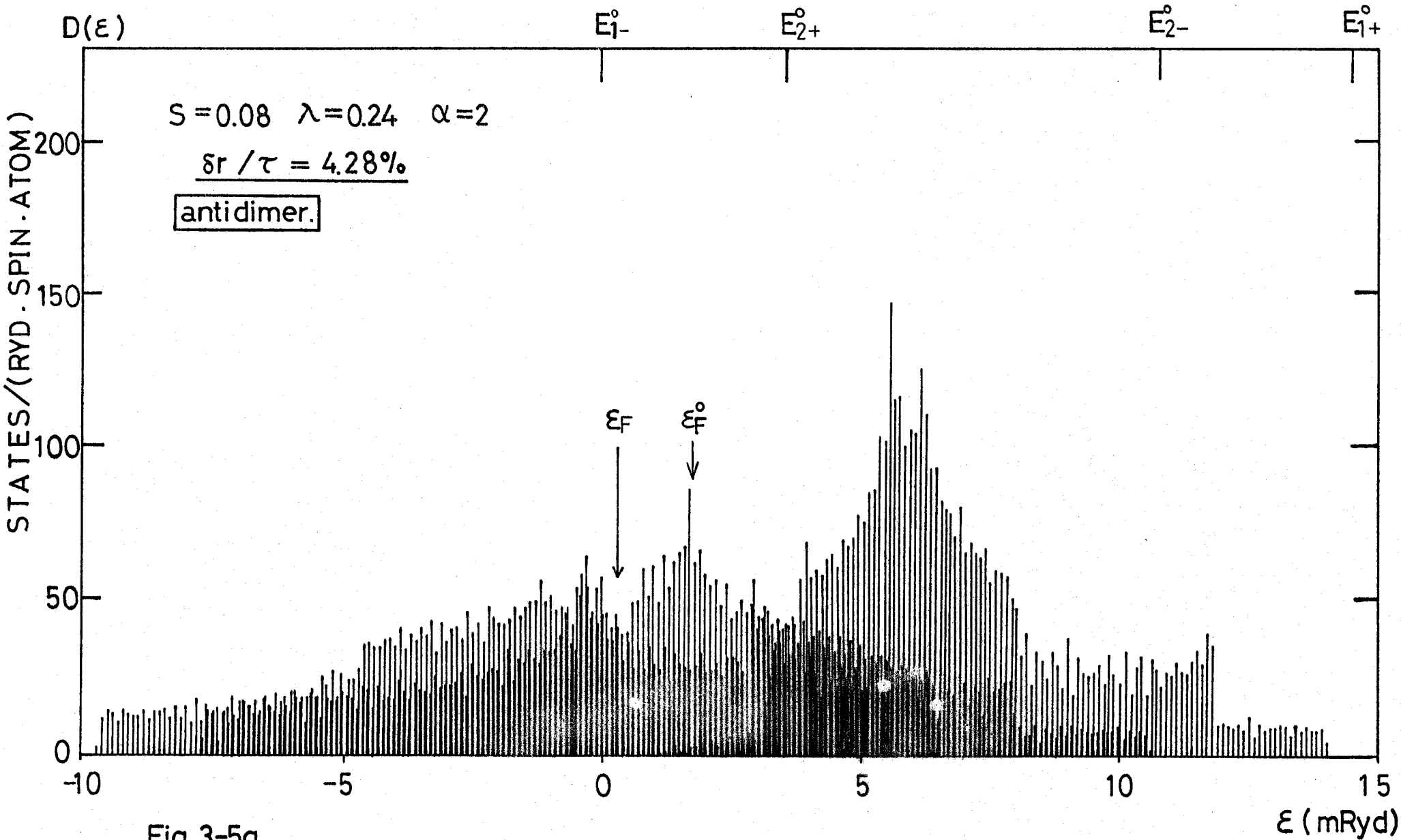
D(ε)
E°1-
E°2+
E°2-
E°1+
S = 0.08 λ = 0.24 α = 2
δr / τ = 4.28%
antidimer.
STATES/(RYD. SPIN. ATOM)
200
150
100
50
0
εF
ε°F
-10
-5
0
5
10
15
ε (mRyd)

Fig. 3-5a

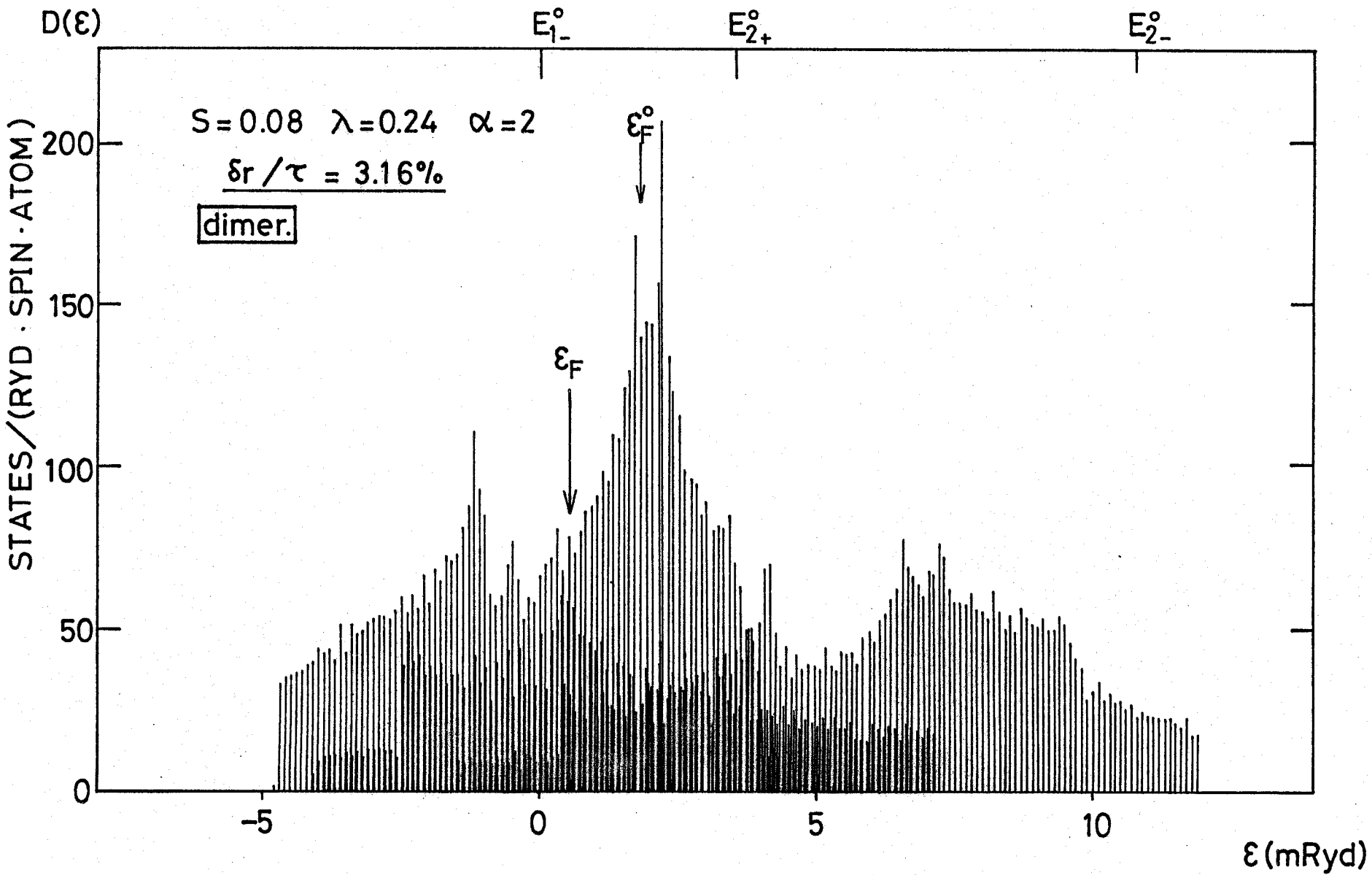
D(ε)
E°_{1-}
E°_{2+}
E°_{2-}
S = 0.08 λ = 0.24 α = 2
δr / τ = 3.16%
dimer.
ε°_F
ε_F
STATES/(RYD · SPIN · ATOM)
200
150
100
50
0
−5
0
5
10
ε (mRyd)

Fig.3-5b

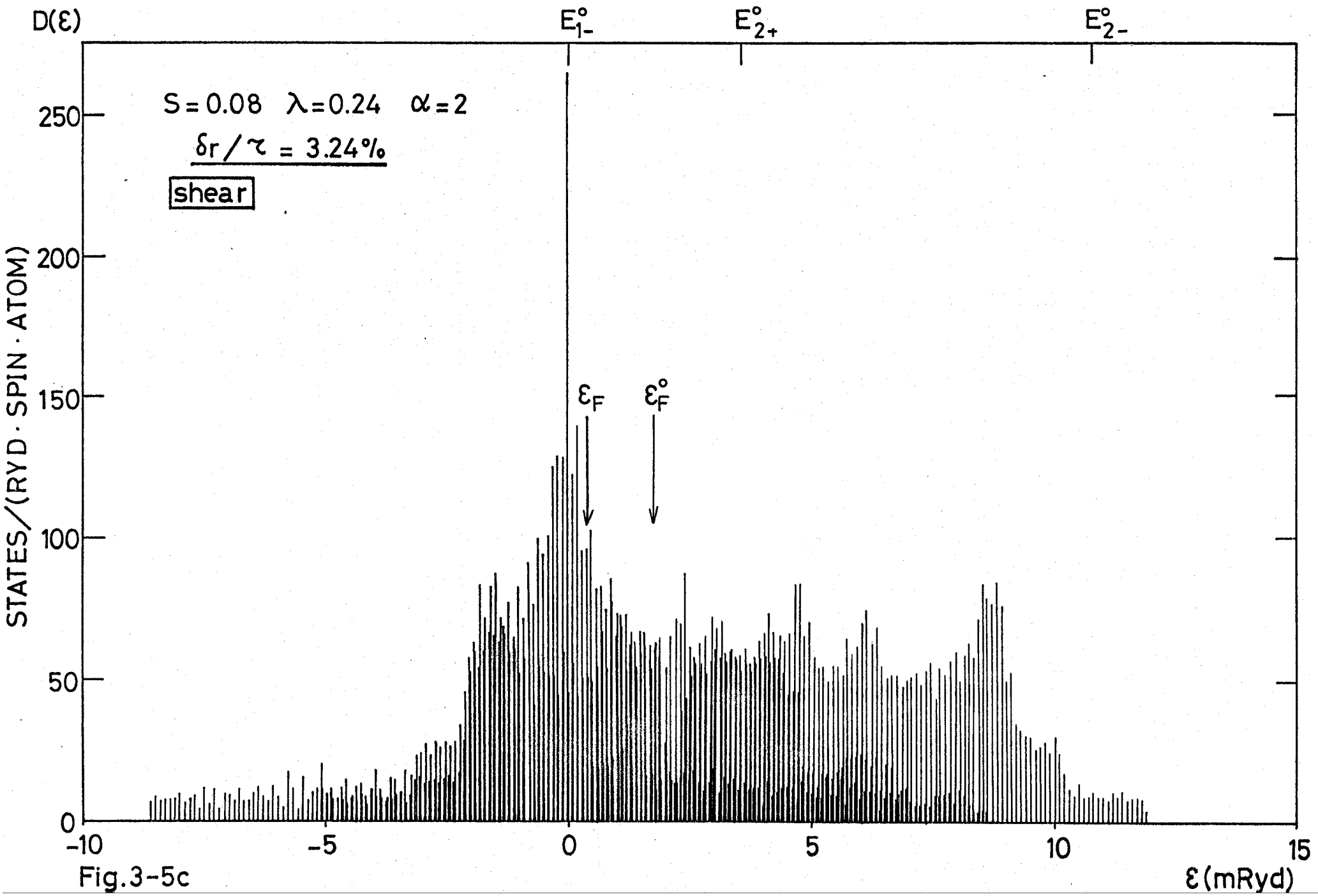
D(ε)
E°_{1-}
E°_{2+}
E°_{2-}
S = 0.08 λ = 0.24 α = 2
δr / τ = 3.24%
shear
ε_F
ε°_F
STATES/(RYD · SPIN · ATOM)
250
200
150
100
50
0
-10
-5
0
5
10
15
ε(mRyd)

Fig.3-5c

§4. Phase Transition

Under the assumption of a small distortion of the Ti^{3+} lattice, the energy change of the k-state of the ith band can be written as

$$E_{ik} = E_i^{(0)} + \delta r g_{ik}. \tag{4.1}$$

The Helmholz free energy is given by

$$F = c\delta r^2/2 + \mu N_{el} - k_B T \sum_{i,k} \ln[1 + \exp\{(\mu - E_{ik})/k_B T\}], \tag{4.2}$$

where N_{el} is the total number of electrons and μ is the chemical potential, and c is elasticity constant. From $\partial F/\partial \delta r = 0$ and $\partial F/\partial \mu = 0$, we obtain

$$\delta r = -\frac{1}{c} \sum_{i,k} g_{ik} f(E_{ik}), \tag{4.3}$$

and

$$N_{el} = \sum_{i,k} f(E_{ik}), \tag{4.4}$$

where $f(E_{ik})$ is the Fermi distribution function. Eqs. (4.3) and (4.4) are the self-consistency equations to determine both δr and μ as functions of temperature. By taking the limit of $\delta r = 0$ in Eq. (4.3) we obtain the equation determining the transition point T_c:

$$\begin{aligned} k_B T_c &= \frac{1}{c} \sum_i f(E_i^{(0)}, T_c)[1 - f(E_i^{(0)}, T_c)] \sum_k g_{ik}^2, \\ f(E_i^{(0)}, T_c) &= 1/[\exp\{(E_i^{(0)} - \mu^{(0)})/k_B T_c\} + 1], \end{aligned} \tag{4.5}$$

where $\mu^{(0)}$ denotes the chemical potential in the undistorted lattice. In the derivation of this equation we used the relation

$$\sum_k g_{ik} = 0, \tag{4.6}$$

which is satisfied for each band i.

At the zero of temperature the total energy in the distorted lattice measured from that in the undistorted lattice is given by

$$E_{tot} = \sum_{i,k} [E_{ik} f(E_{ik}) - E_{ik}^{(0)} f(E_{ik}^{(0)})] + c\delta r^2/2, \tag{4.7}$$

where the first and the second terms are the electronic and lattice energies, respectively. Within the approximation of taking intra-band elements and linear terms in δr, the center of each band in the distorted lattices unchanges, since Eq. (4.6) holds good. As mentioned in §3, for δr smaller than δr_c there is no change of the electronic energy due to the distortion and the total energy increases as a function of δr, which is given by $c\delta r^2/2$. For δr larger than δr_c there is a decrease of the electronic energy which can be written approximately as $b(\delta r - \delta r_c)$, where b and δr_c are determined by S' and γ' and the additional overlap and transfer integrals together with S and γ. Therfore, if c is smaller than $b/2\delta r_c$, the total energy as a function of δr shows a behavior described by the curve (a) in Fig. 4-1. Namely one maximum and one minimum exist and the latter corresponds to an equilibrium

displacement at 0 K. When c equals to $b/2\delta r_c$ the total energy becomes as the curve (b) in Fig. 4-1. In the cace of $c>b/2\delta r_c$ the total energy has the lowest value at $\delta r=0$ and therefore the undistorted structure is most stable. With the aid of the group theoretical consideration given in Appendix 4 we find that the three types of lattice distortion considered here correspond to a phonon mode at the zone-center. So that c is related to the phonon frequency. In fact, as discussed in detail in Appendix 3, we obtain the relation

$$c = 2NM\omega_0^2, \tag{4.8}$$

where M is the mass of Ti ion, ω_0 the phonon frequency and N the number of unit cells. Using Eq. (4.8), we actually calculated the total energy as a function of $\delta r/\tau$ (τ is the distance between n.n. Ti^{3+}ions), assuming the following values of the parameters: S = 0.07, 0.08, 0.09, and 0.10, $\lambda = 3S$, $\alpha = 2$, and $\omega_0 = 130cm^{-1}$. The results are shown in Fig. 4-2. Comparing the minimum energies of the antidimerization, the dimerization, and the shear, we concluded that the antidimerization is most stable at the zero temperature.

At finite temperatures we must solve the self-consistency equations (4.3) and (4.4) to determine δr and the chemical potential μ. Assuming the same parameters as those used in the above calculation we obtained two solutions for δr, except

$\delta r = 0$, in the low temperature range $0<T<T_c'$(see Fig. 4-3). The smaller one corresponds to a maximum free energy and the larger one to a minimum free energy. For $T_c'<T<T_c$ we obtain only one self-consistent solution for δr which gives a minimum free energy. For $T>T_c$ there exists no self-consistent solution except $\delta r = 0$. The temperature T_c corresponds to the second order transition point. If we plot the free energy as a function of δr, it will vary with temperature as shown in Fig. 4-4. We verified such temperature variation of the free energy by calculating the temperature dependence of the second derivative of the free energy at $\delta r = 0$. The calculated equilibrium displacements that give the minimum free energy are plotted in Fig. 4-5 as functions of temperature. If we plot δr normalized by its value at 0 K as a function of normalized temperature T/T_c, we obtain the almost similar curves for the cases of S = 0.07, 0.08, 0.09, and 0.10. Both the anti-dimerization and the dimerization have the same transition point, because the expression of g_{ik} for the former differs only in its sign from that for the latter and T_c depends on $(g_{ik})^2$. The transition temperature for these two types of distortion is higher than that for the shear. $\delta r_c/\tau$, $\delta r(T=0)/\tau$, and T_c are listed in Table 4-1. For fixed values of the tight-binding parameters we have a critical phonon frequency ω_c that gives the upper limit of the instability condition, which is given approximately by $c=b/2\delta r_c$. ω_c is also listed in Table 4-1.

Table 4-1

$\lambda = 3S$, $\alpha = 2$, $S' = 0.065(\text{a.u.})^{-1}$, $\omega_0 = 130\text{cm}^{-1}$.

Antidimerization

S	$\delta r_c/\tau$	$\delta r(T=0)/\tau$	T_c	T_c'	ω_c
0.07	0.74 %	3.43 %	235 K	85 K	146 cm^{-1}
0.08	0.84	4.28	355	105	152
0.09	0.95	5.10	507	138	157
0.10	1.07	6.04	715	175	166

Dimerization

S	$\delta r_c/\tau$	$\delta r(T=0)/\tau$	T_c	T_c'	ω_c
0.07	0.65 %	2.59 %	235 K	85 K	139 cm^{-1}
0.08	0.75	3.16	355	105	143
0.09	0.84	3.84	507	138	145
0.10	0.94	4.68	715	175	150

Shear

S	$\delta r_c/\tau$	$\delta r(T=0)/\tau$	T_c	T_c'	ω_c
0.07	0.59 %	2.63 %	218 K	87 K	136 cm^{-1}
0.08	0.67	3.24	322	115	139
0.09	0.76	3.93	465	145	143
0.10	0.84	4.76	657	182	146

Figure Captions

Fig. 4-1. Plot of the total energy as a function of δr. The broken lines and the dotted curve show the energy gain in the electron system and the lattice energy, respectively.

Fig. 4-2. The total energy change vs. $\delta r/\tau$ calculated for the three kinds of distorted lattice.

Fig. 4-3. Self-consistent solutions at finite temperatures.

Fig. 4-4. Plot of the free energy as a function of δr and T.

Fig. 4-5. Temperature variation of the equilibrium displacement determined self-consistently.

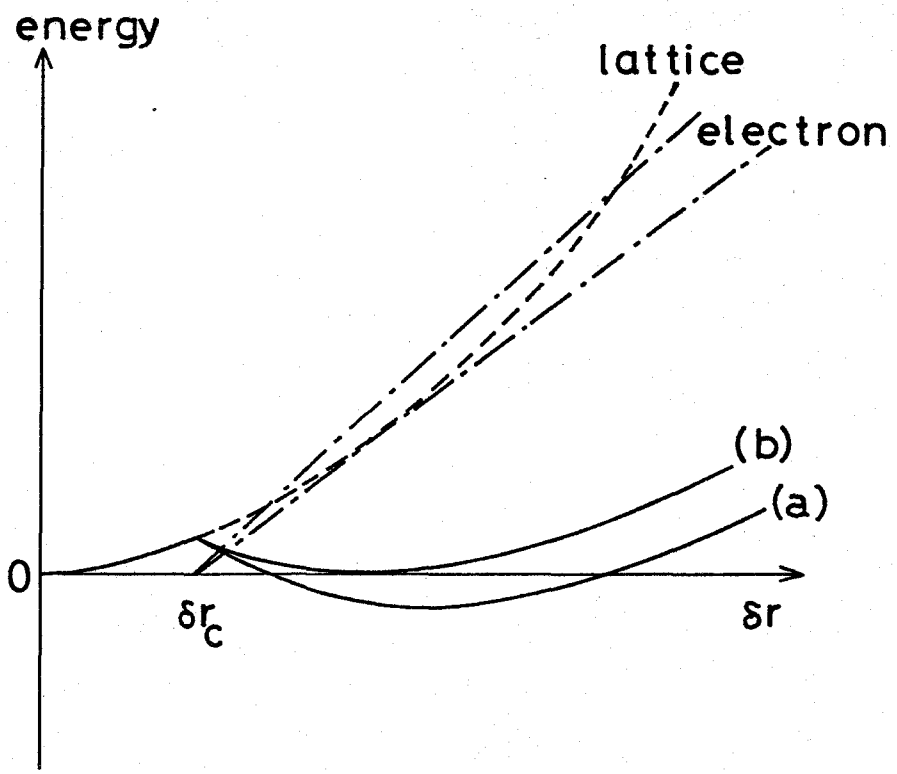

Fig. 4-1

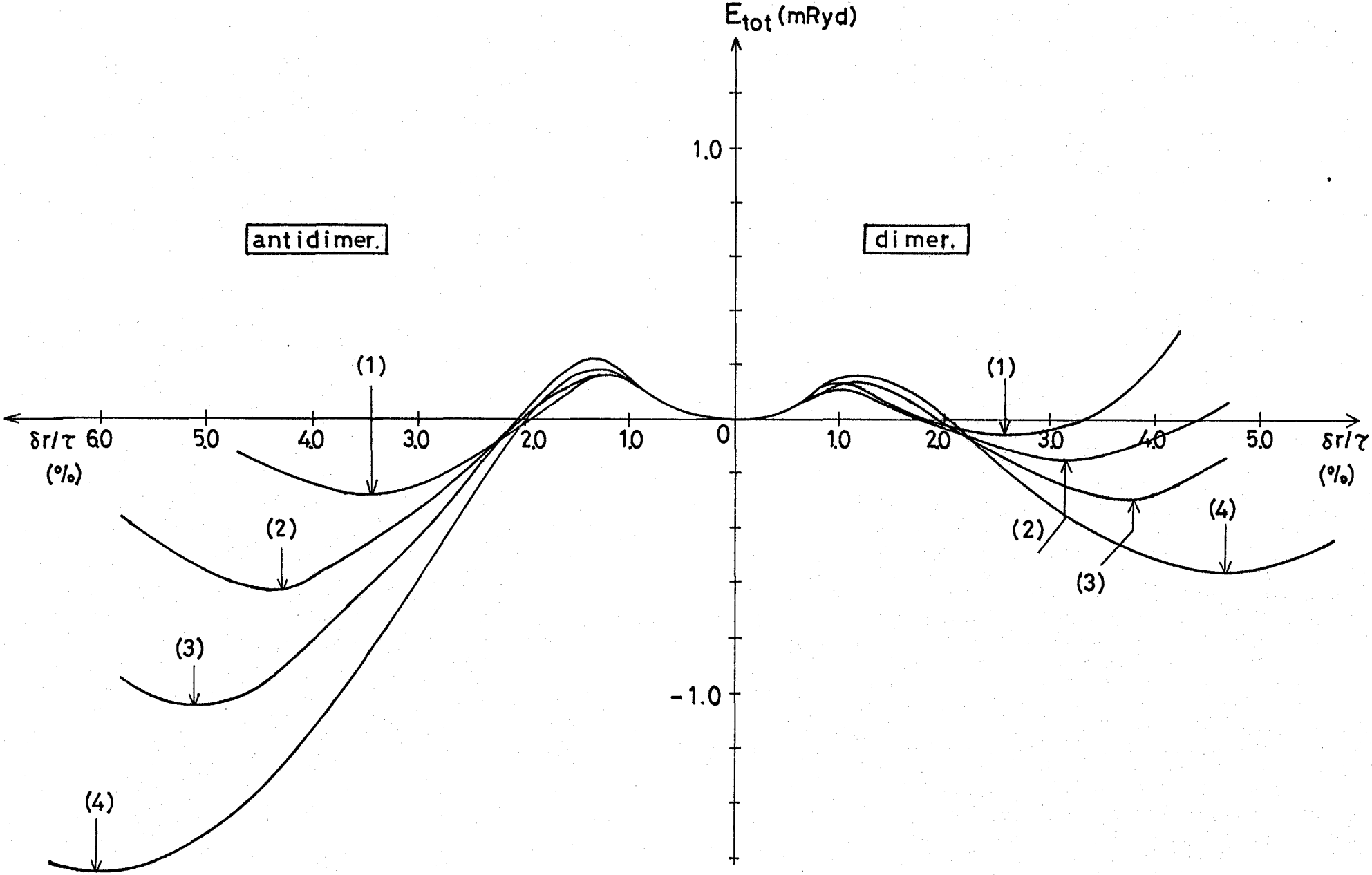
E_{tot} (mRyd)
1.0
-1.0
antidimer.
dimer.
(1)
(2)
(3)
(4)
δr/τ (%)
6.0
5.0
4.0
3.0
2.0
1.0
0
1.0
2.0
3.0
4.0
5.0
δr/τ (%)

Fig. 4-2a

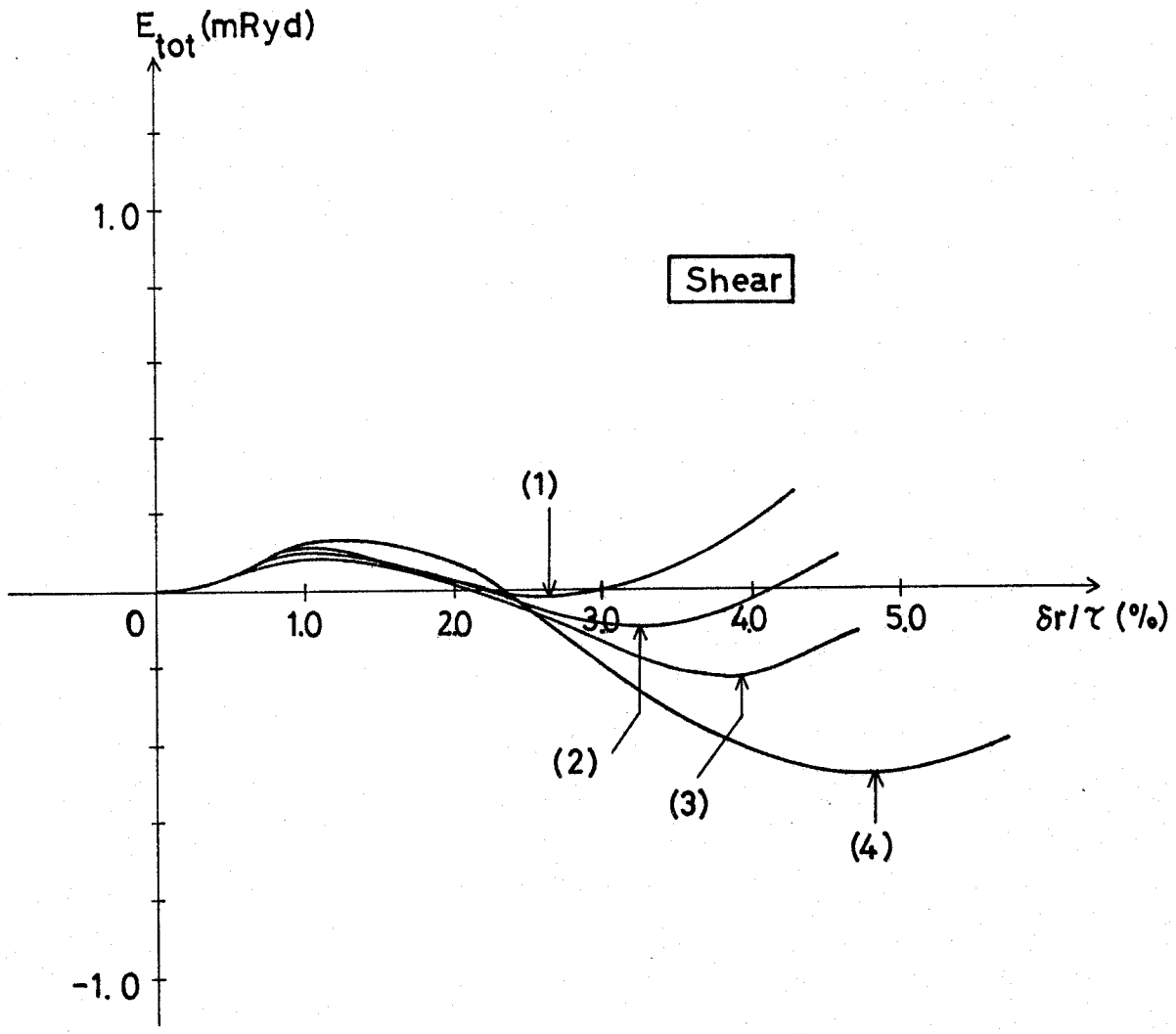

Fig. 4-2b

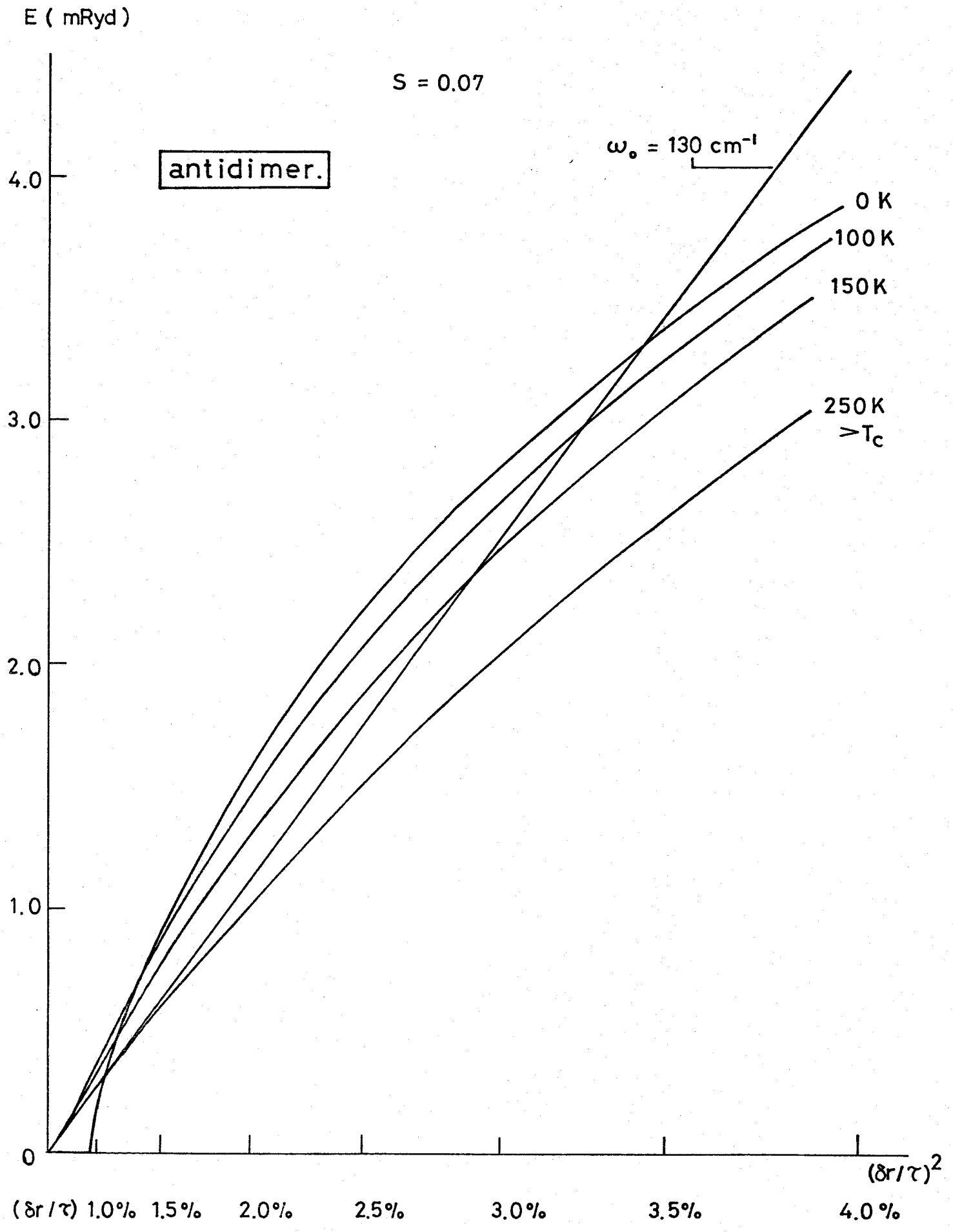
E (mRyd)
S = 0.07
antidimer.
ω_o = 130 cm^{-1}
0 K
100 K
150 K
250 K
$>T_c$
4.0
3.0
2.0
1.0
0
$(\delta r/\tau)^2$
$(\delta r/\tau)$ 1.0% 1.5% 2.0% 2.5% 3.0% 3.5% 4.0 %

Fig. 4-3

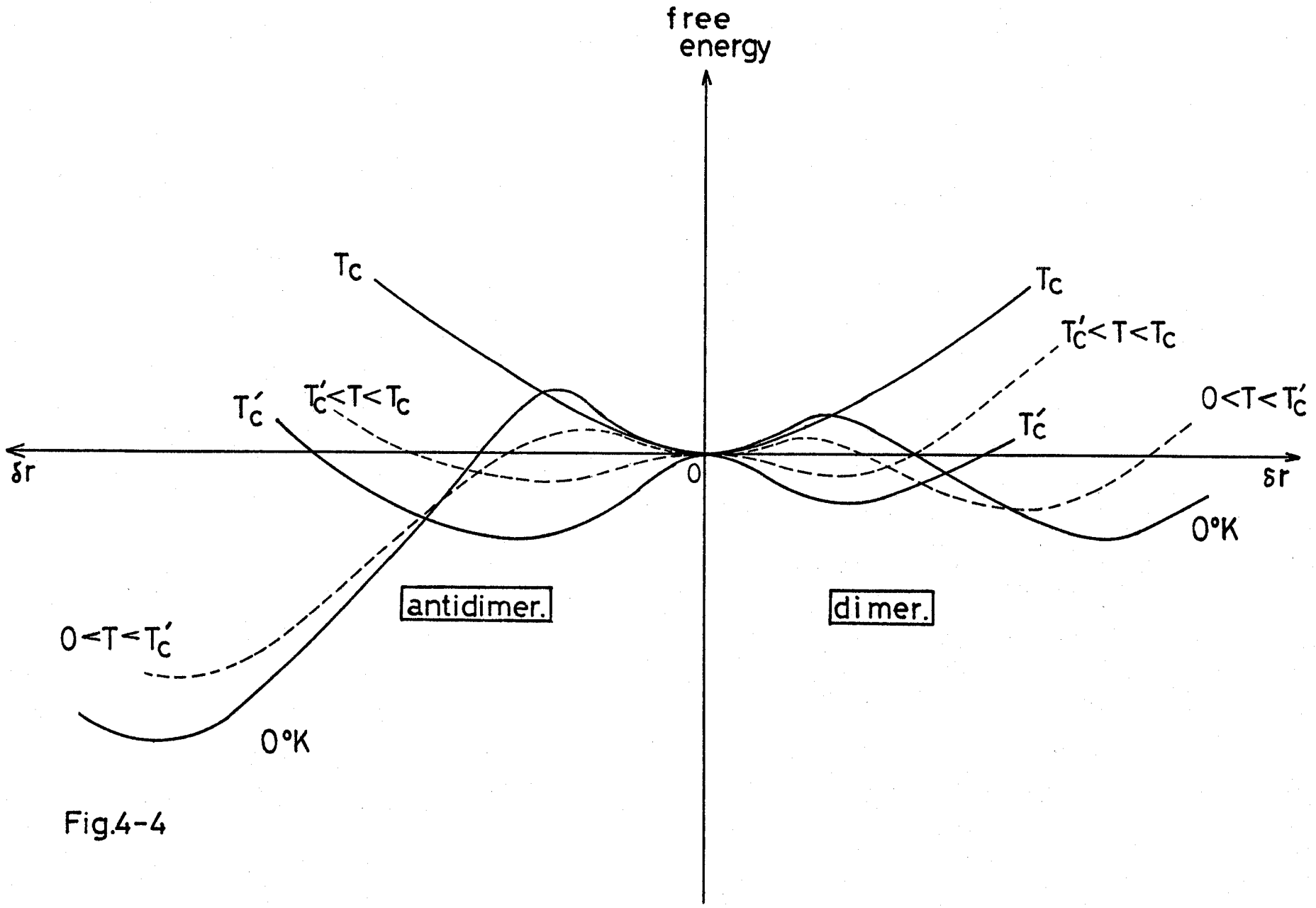
free
energy
Tc
T'c<T<Tc
T'c
0<T<T'c
δr
0
δr
0°K
antidimer.
dimer.
Tc
T'c<T<Tc
T'c
0<T<T'c
0°K

Fig.4-4

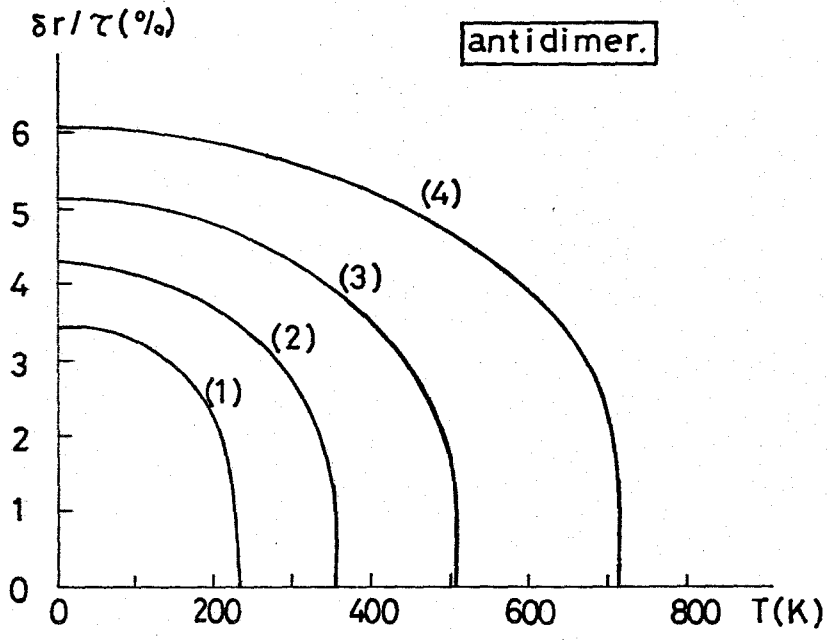

T_c = 235, 355, 507, 715 K

	S
(1)	0.07
(2)	0.08
(3)	0.09
(4)	0.10

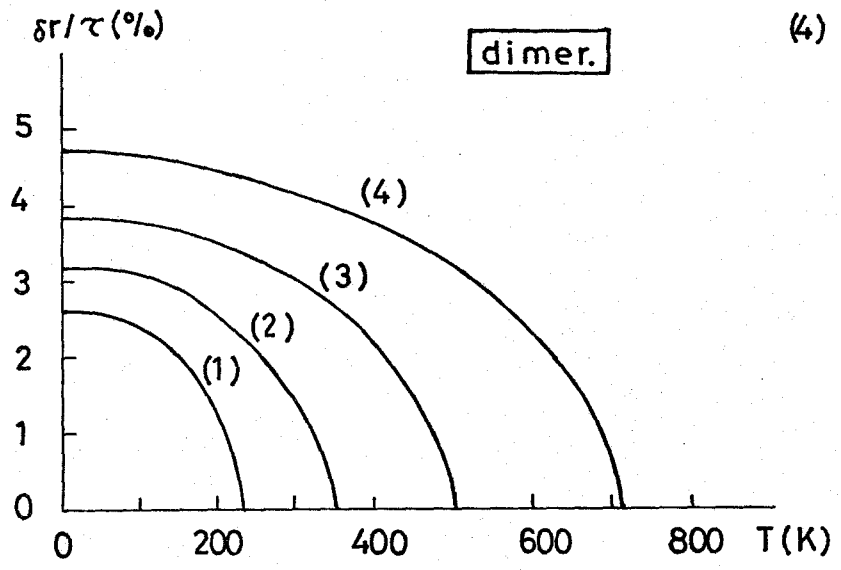

Fig. 4-5

§5. Magnetic Susceptibility

In this section we study temperature variation of the paramagnetic susceptibility due to the phase transition based on our model. The general expression of the paramagnetic susceptibility for band electron is given by

$$\chi(T) = 2\mu_B^2 \frac{1}{k_B T} \int_{-\infty}^{\infty} f(E)[1 - f(E)]\, D(E)\, dE, \tag{5.1}$$

where $f(E)$ is the Fermi distribution function and $D(E)$ denotes the density of states per spin. As obtained in §2, in the undistorted phase there are six dispersionless bands and the density of states are expressed as

$$D(E) = N[\delta(E) + 2\delta(E-\Gamma) + 2\delta(E-3\Gamma) + \delta(E-4\Gamma)], \tag{5.2}$$

where Γ represents the energy separation between the lowest singlet band and the lower doublet band. By inserting Eq.(5.2) into Eq.(5.1), $\chi(T)$ is given by the following expression:

$$\chi(T) = 2N\mu_B^2 \beta x\left[\frac{1}{(1+x)^2} + \frac{2\exp(\Gamma\beta)}{\{1+x\exp(\Gamma\beta)\}^2} + \frac{2\exp(3\Gamma\beta)}{\{1+x\exp(3\Gamma\beta)\}^2} + \frac{\exp(4\Gamma\beta)}{\{1+x\exp(4\Gamma\beta)\}^2}\right], \tag{5.3}$$

where

$$x = \exp(-\mu\beta) \qquad (\beta = 1/k_B T), \tag{5.4}$$

and μ is the chemical potential determined self-consistently by the equation

$$\frac{1}{1+x} + \frac{2}{1+x\exp(\Gamma\beta)} + \frac{2}{1+x\exp(3\Gamma\beta)} + \frac{1}{1+x\exp(4\Gamma\beta)} = 1. \qquad (5.5)$$

In the distorted phase the paramagnetic susceptibility is calculated by Eq.(5.1), using the density of states calculated in §3 and the chemical potential determined self-consistently in §4. Especially at the zero temperature χ is given by the usual expression of the Pauli paramagnetism:

$$\chi(0) = 2N\mu_B{}^2 D(E_F), \qquad (5.6)$$

where $D(E_F)$ is the density of states at the Fermi level.

The susceptibilities calculated above and below T_c are shown in Fig. 5-1 by the full curves. Here we take the antidimerization as the distortion below T_c and the four curves (1), (2), (3), and (4) correspond to the cases of S=0.07, 0.08, 0.09, and 0.1, respectively. For comparison, we also calculate the susceptibilities below T_c with the use of Eq.(5.3) which is useful only above T_c, and show the results by the dotted curves in Fig. 5-1. The measured one is shown by the broken curve. As observed by Ogawa, the lattice constant a varies with temperature and especially near T_c it increases abruptly with increasing temperature. Such effect can be taken into account by using the different values of the overlap integral S for each region below and above T_c. Therefore if we consider that the susceptibilities below and above T_c are given by the curve (4) and the curve (1), respectively, we can explain qualitatively the observed temperature dependence of the susceptibility.

Figure Captions

Fig. 5-1. Temperature variation of the paramagnetic susceptibility. The full curves show the calculated results for the undistorted structure above T_c and for the antidimerized structure below T_c. The susceptibility for the undistorted lattice varies with temperature below T_c as shown by the dotted curves. The broken curve shows the experimental result.

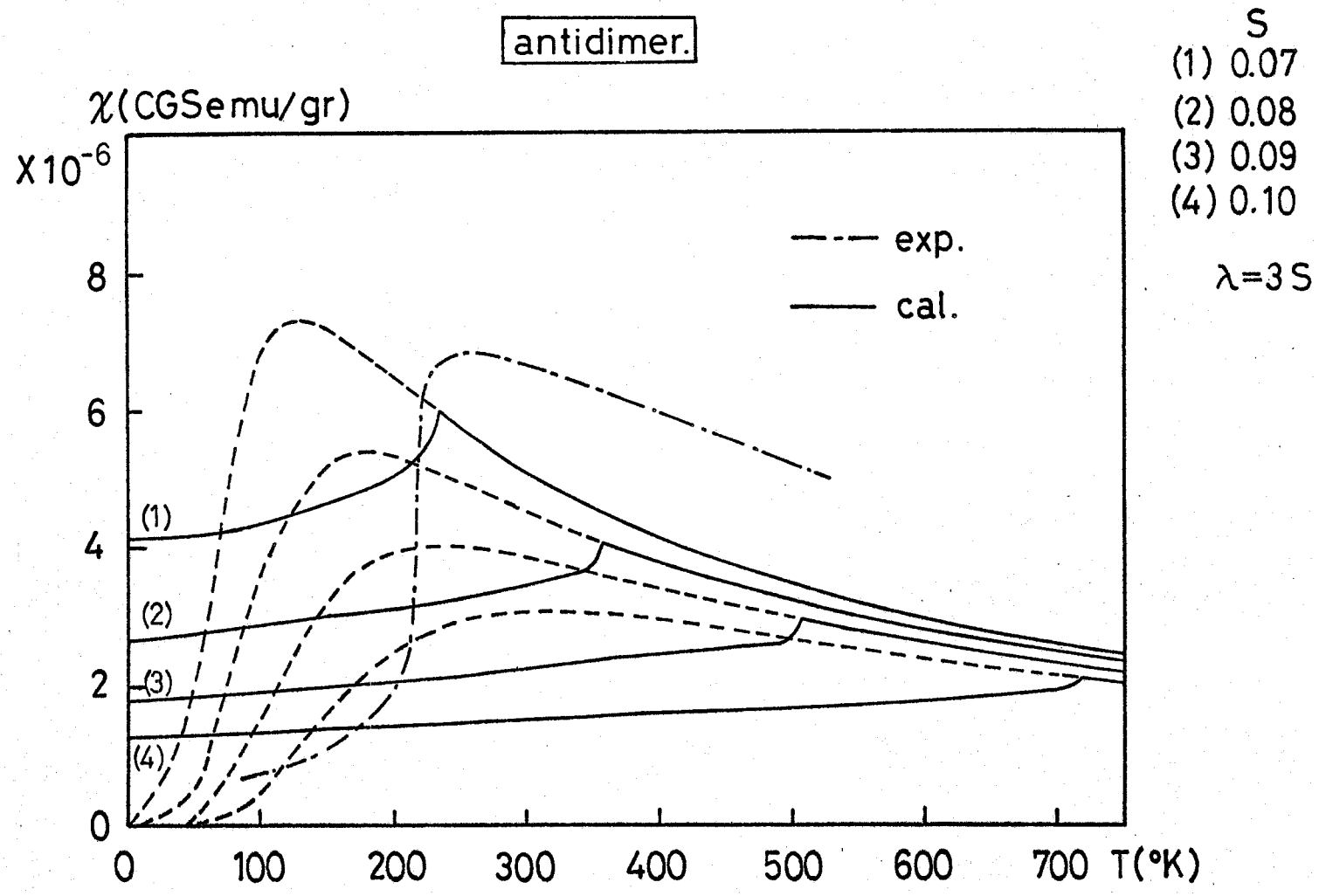
antidimer.
χ(CGSemu/gr)
X10⁻⁶
8
6
4
2
0
exp.
cal.
(1)
(2)
(3)
(4)
0
100
200
300
400
500
600
700
T(°K)
S
(1) 0.07
(2) 0.08
(3) 0.09
(4) 0.10
λ=3S

Fig.5-1a

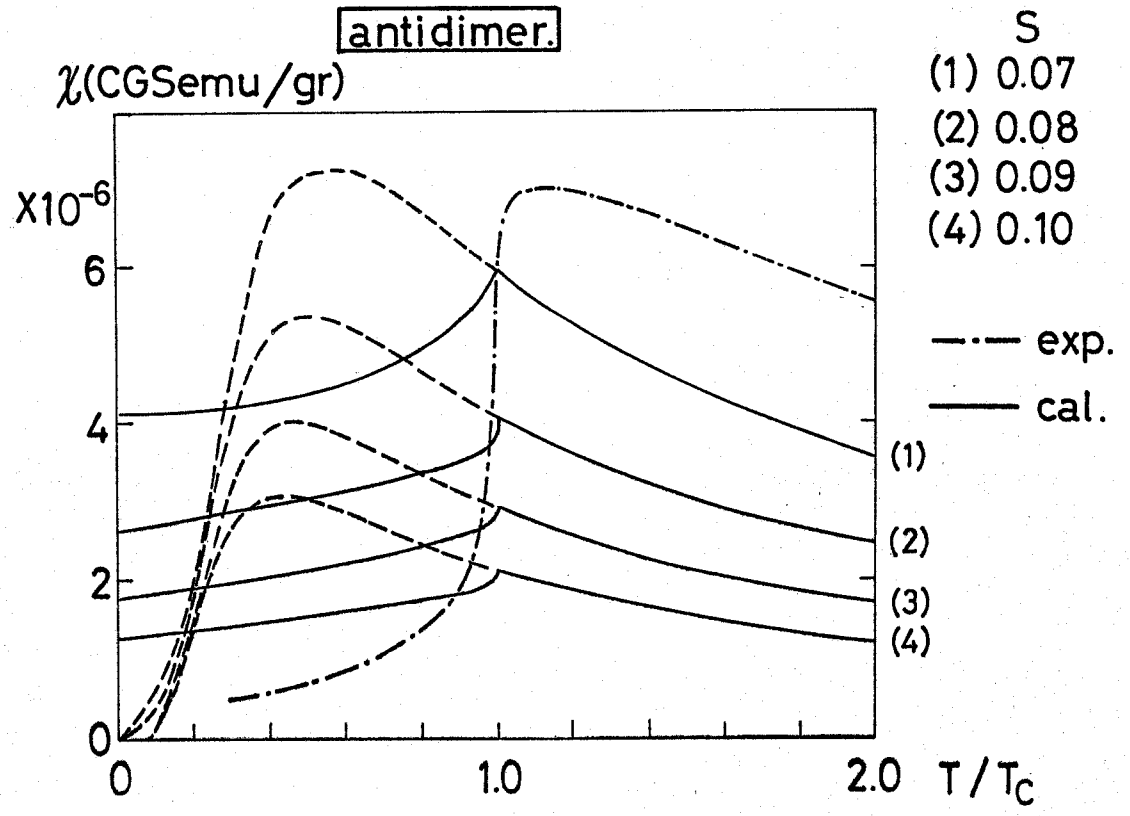
antidimer.
χ(CGSemu/gr)
X10⁻⁶
6
4
2
0
0
1.0
2.0
T/Tc
S
(1) 0.07
(2) 0.08
(3) 0.09
(4) 0.10
exp.
cal.
(1)
(2)
(3)
(4)

Fig.5-1b

§6. Discussion

a) Possibility of superlattice structure

Now we are concerned with such a lattice distortion that changes the lattice periodicity, but preserves inversion symmetry. Refferring to Appendix 4, we find that the corresponding phonon modes that satisfy the above requirements are those at zone-boundary M points only, and have wavevector $\mathbf{Q}=\pm\mathbf{a}^*/2$, $\pm\mathbf{b}^*/2$, and $\pm(\mathbf{a}^*\pm\mathbf{b}^*)/2$. Again, confining ourselves to the displacement of Ti ions parallel to their sheet, we obtain two kinds of the independent M point mode. Both of them belong to A_g irreducible representation of this point. The lattice periodicity modulated by these modes becomes two times larger than the basic periodicity in the direction of either or both of the basis vectors. In order to examine whether the lattice distortions corresponding to M point modes occur or not, we calculated the transition point for these types of distortion on the basis of Eq. (4.5). If we assume the same phonon frequency as that for Γ point E_g mode discussed in §§3 and 4, the transition point was not found at finite temperatures. In general the phonon frequency for A_g mode at M point may differ from that for E_g mode at the zone-center. Therefore we examined the maximum phonon frequency for M point A_g modes, which defines the upper limit of the instability criterion, and found that it was much lower than that for Γ point E_g mode. Then, at the present stage, we may conclude that the electron-lattice coupled system is most stabilized by the lattice distortion of the antidimerization type, if the phase transition occurs.

b) Effect of interband mixing

In this paper we have studied the effect of the intraband mixing only, namely the band overlapping resulting from the splitting of the doublet bands and the broadening of each band. However, when two bands happen to cross at a certain point in the Brillouin zone, the interband coupling will bring in an energy gap between the two bands around the cross point. In order to determine the energy gap, however, we must solve the seqular equation exactly. Although we have not yet carried out the exact calculation, from the dispersion curves obtained in §3, we can imagine that the band crossing arises along lines in the k-space, and along them energies remarkably change. Then if we count the number of Bloch states that fall into a limited energy range, we will see that the crossing points are only their minority, if included, and among their majority the interband mixing does not exist. Furthermore, since this interband effect causes a repulsion between the energy of the lowest singlet band and that of the excited doublet band, the total energy in the distorted lattice becomes lower than that calculated in this paper. Namely, the interband effect also contributes to the stabilization of the distorted lattice. Thus we can expect that the results obtained in this paper is not affected in essence by the interband effect.

c) Effect of electron correlation

In this paper we have neglected effects of the electron correlation.

We may only expect that the correlation effects enhance the paramagnetic susceptibility above the transition temperature, because the $3d\varepsilon$ bands in the undistorted lattice are quite narrow. It is a difficult and further problem to examine the effects of the electron correlation on the phase transition in the electron-lattice coupled system.

References

1) S. Ogawa: J. Phys. Soc. Japan 15, 1901 (1960).

2) F. Cavallone, I. Pollini, and G. Spinolo: Lettere al Nuovo Cimento 4, 764 (1970).

3) F. Cavallone, I. Pollini, and G. Spinolo: Phys. Status solidi (b) 45, 405 (1971).

4) C.A. Emeis, F.J. Reinders, and E. Drent: Solid State Commun.: 16, 239 (1975).

5) R.E. Watson: Phys. Rev. 118, 1036 (1960).

Appendix 1. Matrix Element of $K_{pd}^{(0)} + \Delta K_{pd}$

We show the matrix elements of $K_{pd}^{(0)} + \Delta K_{pd}$ in Table A1. Here the displacement vector of μth Ti ion (μ=I,II) is written as

$$\vec{\delta r}_\mu = \delta r \ (x_\mu, y_\mu, z_\mu), \tag{A1.1}$$

where x_μ, y_μ, and z_μ denote the direction cosines of $\vec{\delta r}_\mu$ with respect to the local principal axes. We set

for antidimerization

$$\vec{\delta r}_I = \delta r(1/\sqrt{2}, -1/\sqrt{2}, 0) = -\vec{\delta r}_{II}, \tag{A1.2}$$

for dimerization

$$\vec{\delta r}_I = \delta r(-1/\sqrt{2}, 1/\sqrt{2}, 0) = -\vec{\delta r}_{II}, \tag{A1.3}$$

for shear

$$\vec{\delta r}_I = \delta r(-1/\sqrt{6}, -1/\sqrt{6}, 2/\sqrt{6}) = -\vec{\delta r}_{II}. \tag{A1.4}$$

We write

$$\Delta_0 = \gamma - ES, \tag{A1.5}$$

$$\begin{aligned} \Delta &= \gamma' - ES', \\ \sigma &= \gamma'_\sigma - ES'_\sigma, \\ \Pi &= \gamma'_\pi - ES'_\pi. \end{aligned} \tag{A1.6}$$

The phase factors are defined as follows:

$$e_i = \exp(ik\cdot\tau_i), \qquad e_{ij} = \exp[ik\cdot(\tau_i-\tau_j)/3], \quad (i,j = 1, 2, 3) \tag{A1.7}$$

where τ_i is a vector that joins ith nearest neighbor pair of Ti ions. e_i and e_{ij} come from the phase factor of the dε Bloch function and that of the 3p Bloch function, respectively.

Table A1 $K_{pd} \equiv K_{pd}^{(0)} + \Delta K_{pd}$:

	ξ_I	η_I	ζ_I	ξ_{II}	η_{II}	ζ_{II}
p_{1x}		$e_{13}\sigma z_I$	$e_{13}\sigma y_I$		$e_{13}e_3[\Delta_0+\Delta z_{II}]$	$-e_{13}e_3\Pi y_{II}$
p_{1y}	$-e_{13}\Pi z_I$		$e_{13}[\Delta_0+\Delta x_I]$	$e_{13}e_3[\Delta_0+\Delta z_{II}]$		$-e_{13}e_3\Pi x_{II}$
p_{1z}	$-e_{13}\Pi y_I$	$e_{13}[\Delta_0+\Delta x_I]$		$e_{13}e_3\sigma y_{II}$	$e_{13}e_3\sigma x_{II}$	
p_{2x}		$-e_{23}[\Delta_0-\Delta z_I]$	$-e_{23}\Pi y_I$		$e_{23}e_3\sigma z_{II}$	$e_{23}e_3\sigma y_{II}$
p_{2y}	$-e_{23}[\Delta_0-\Delta z_I]$		$-e_{23}\Pi x_I$	$-e_{23}e_3\Pi z_{II}$		$-e_{23}e_3[\Delta_0-\Delta x_{II}]$
p_{2z}	$e_{23}\sigma y_I$	$e_{23}\sigma x_I$		$-e_{23}e_3\Pi y_{II}$	$-e_{23}e_3[\Delta_0-\Delta x_{II}]$	
p_{3x}		$e^*_{23}[\Delta_0+\Delta z_I]$	$-e^*_{23}\Pi y_I$		$-e^*_{23}e_2\Pi z_{II}$	$e^*_{23}e_2[\Delta_0+\Delta y_{II}]$
p_{3y}	$e^*_{23}[\Delta_0+\Delta z_I]$		$-e^*_{23}\Pi x_I$	$e^*_{23}e_2\sigma z_{II}$		$e^*_{23}e_2\sigma x_{II}$
p_{3z}	$e^*_{23}\sigma y_I$	$e^*_{23}\sigma x_I$		$e^*_{23}e_2[\Delta_0+\Delta y_{II}]$	$-e^*_{23}e_2\Pi x_{II}$	
p_{4x}		$-e_{12}\Pi z_I$	$-e_{12}[\Delta_0-\Delta y_I]$		$-e_{12}e_2[\Delta_0-\Delta z_{II}]$	$-e_{12}e_2\Pi y_{II}$
p_{4y}	$e_{12}\sigma z_I$		$e_{12}\sigma x_I$	$-e_{12}e_2[\Delta_0-\Delta z_{II}]$		$-e_{12}e_2\Pi x_{II}$
p_{4z}	$-e_{12}[\Delta_0-\Delta y_I]$	$-e_{12}\Pi x_I$		$e_{12}e_2\sigma y_{II}$	$e_{12}e_2\sigma x_{II}$	
p_{5x}		$-e^*_{12}\Pi z_I$	$e^*_{12}[\Delta_0+\Delta y_I]$		$e^*_{12}e_1\sigma z_{II}$	$e^*_{12}e_1\sigma y_{II}$
p_{5y}	$e^*_{12}\sigma z_I$		$e^*_{12}\sigma x_I$	$-e^*_{12}e_1\Pi z_{II}$		$e^*_{12}e_1[\Delta_0+\Delta x_{II}]$
p_{5z}	$e^*_{12}[\Delta_0+\Delta y_I]$	$-e^*_{12}\Pi x_I$		$-e^*_{12}e_1\Pi y_{II}$	$e^*_{12}e_1[\Delta_0+\Delta x_{II}]$	
p_{6x}		$e^*_{13}\sigma z_I$	$e^*_{13}\sigma y_I$		$-e^*_{13}e_1\Pi z_{II}$	$-e^*_{13}e_1[\Delta_0-\Delta y_{II}]$
p_{6y}	$-e^*_{13}\Pi z_I$		$-e^*_{13}[\Delta_0-\Delta x_I]$	$e^*_{13}e_1\sigma z_{II}$		$e^*_{13}e_1\sigma x_{II}$
p_{6z}	$-e^*_{13}\Pi y_I$	$-e^*_{13}[\Delta_0-\Delta x_I]$		$-e^*_{13}e_1[\Delta_0-\Delta y_{II}]$	$-e^*_{12}e_1\Pi x_{II}$	

Appendix 2. Matrix Element of ΔK_{dd}^{eff}

We write the matrix elements of ΔK_{dd}^{eff} as follows:

$$\Delta K_{dd}^{eff}(E,k:\delta r) = .(\gamma - ES)/E$$

$$\begin{array}{c} \\ \Psi_{1-}(k) \\ \Psi_{2a+}(k) \\ \Psi_{2b+}(k) \\ \Psi_{2a-}(k) \\ \Psi_{2b-}(k) \\ \Psi_{1+}(k) \end{array} \begin{array}{c} \begin{array}{cccccc} \Psi_{1-}(k) & \Psi_{2a+}(k) & \Psi_{2b+}(k) & \Psi_{2a-}(k) & \Psi_{2b-}(k) & \Psi_{1+}(k) \end{array} \\ \left(\begin{array}{cccccc} M_{-} & M_{-+}^{a} & M_{-+}^{b} & M_{--}^{a} & M_{--}^{b} & M_{-+} \\ & M_{+}^{aa} & M_{+}^{ab} & M_{+-}^{aa} & M_{+-}^{ab} & M_{++}^{a} \\ & & M_{+}^{bb} & M_{+-}^{ba} & M_{+-}^{bb} & M_{++}^{b} \\ & & & M_{-}^{aa} & M_{-}^{ab} & M_{-+}^{\prime a} \\ & & & & M_{-}^{bb} & M_{-+}^{\prime b} \\ & & & & & M_{+} \end{array} \right), \end{array} \qquad \text{(A2.1)}$$

where each element is a function of wavevector k, energy E, and displacement δr. The energy dependence of the element arises from the first order derivatives of the transfer energy of the form

$$\begin{aligned} \Delta(E) &= \gamma' - ES', \\ \sigma(E) &= \gamma'_{\sigma} - ES'_{\sigma}, \\ \Pi(E) &= \gamma'_{\pi} - ES'_{\pi}. \end{aligned} \qquad \text{(A2.2)}$$

Also the wavevector dependent functions are introduced as follows:

$$f_1(k) = (1/3)\cos 3x_1, \qquad f_{2\pm}(k) = (1/3)(\cos 3x_2 \pm \cos 3x_3),$$

$$g_1(k) = (1/3)\cos x_{23}, \qquad g_{2\pm}(k) = (1/3)(\cos x_{31} \pm \cos x_{12}),$$

$$h_{\pm}(k) = (1/3)(\cos 3x_2 \pm \omega \cos 3x_3),$$

$$f_1'(k) = -(1/3)\sin 3x_1, \qquad f_{2\pm}'(k) = -(1/3)(\sin 3x_2 \pm \sin 3x_3),$$

$$g_1'(k) = -(1/3)\sin x_{23}, \qquad g_{2\pm}'(k) = -(1/3)(\sin x_{31} \pm \sin x_{12}),$$

$$h_\pm'(k) = -(1/3)(\sin 3x_2 \pm \omega \sin 3x_3), \qquad \text{(A2.3)}$$

where $\omega = \exp(2\pi i/3)$, $x_i = k\cdot\tau_i$, $x_{ij} = k\cdot(\tau_i - \tau_j)$ $(i,j = 1,2,3)$, and τ_i is a vector that joins ith nearest neighbor pair of Ti ions.

With the use of Eq.(A2.2) and Eq.(A2.3) one obtains the explicit expression of the element:

intraband elements for antidimerization

$$M_\pm(E,k;\delta r) = \pm\sqrt{2}\delta r[\sigma(E)\{2f_1(k) - f_{2+}(k) - 2g_1(k) + g_{2+}(k)\} - \Pi(E)\{2g_1(k) - g_{2+}(k)\}],$$

$$M_\pm^{aa}(E,k;\delta r) = M_\pm^{bb}(E,k;\delta r) = \pm\sqrt{2}\delta r[\sigma(E)\{2f_1(k) - f_{2+}(k) + g_1(k) - g_{2+}(k)/2\} - \Pi(E)\{2g_1(k) - g_{2+}(k)\}],$$

$$M_\pm^{ab}(E,k;\delta r) = \pm\sqrt{2}\delta r[\sigma(E)(\omega^2\{2f_1(k) + g_1(k) + g_{2+}(k)\} - h_+(k)) + \Pi(E)\omega^2\{g_1(k) + g_{2+}(k)\} - \Delta(E)\omega^2], \qquad \text{(A2.4)}$$

interband elements for antidimerization

$$M_{-+}^{a}(E,k;\delta r) = -i\sqrt{2}\delta r[\sigma(E)\{(1-\omega)\, g_1'(k)/2 + \omega^2 g_{2-}'(k)/2 - 2\omega^2 f_1'(k) + h_+'(k)\} + \Pi(E)\{(1-\omega)g_1'(k) + \omega^2 g_{2-}'(k)\}],$$

$$M_{-+}^{b}(E,k;\delta r) = -i\sqrt{2}\delta r[\text{ c.c. of the above }]. \qquad \text{(A2.5)}$$

Here we considered the elements among the first singlet band and

the first doublet band.

intraband elements for shear

$$M_{\pm}(E,k;\delta r) = \pm\sqrt{6}\delta r[\sigma(E)\{g_{2-}(k) - f_{2-}(k)\} + \Pi(E)g_{2-}(k)],$$

$$M_{\pm}^{aa}(E,k;\delta r) = M_{\pm}^{bb}(E,k;\delta r)$$

$$= \pm\sqrt{6}\delta r[\sigma(E)\{f_{2-}(k) - g_{2-}(k)/2\} + \Pi(E)g_{2-}(k)],$$

$$M_{\pm}^{ab}(E,k;\delta r) = \pm\sqrt{6}\delta r[\sigma(E)((1-\omega)/3\{-f_{2-}(k)-g_{2+}(k)\} - h_{-}(k))$$

$$- \Pi(E)(1-\omega)/3\{g_{1}(k) + g_{2+}(k)\} + \Delta(E)(1-\omega)/3]. \qquad \text{(A2.6)}$$

The expression for dimerization is obtained by changing the sign of that for antidimerization. For antidimerization and dimerization we have the following relation among the interband elements:

$$M'^{a}_{-+} = M^{b}_{-+}, \qquad M'^{b}_{-+} = M^{a}_{-+},$$

$$M^{aa}_{+-} = M^{bb}_{+-}, \qquad M^{ab}_{+-} = M^{ba}_{+-}, \qquad \text{(A2.7)}$$

$$M^{a}_{++} = (M^{b}_{++})^{*} = -M^{a}_{--} = -(M^{b}_{--})^{*}.$$

If we take only the intraband elements and consider the energy shift in the $d\varepsilon$ band to first order in δr, we can replace E in the intraband element with each energy eigenvalue in the undistorted phase.

Appendix 3. Electron-Phonon Interaction and Phase Transition

In this appendix we discuss the phase transition on the basis of the electron-phonon interaction. We consider the linear coupling of the electron system discussed in §2 of the text to single phonon mode specified by wavevector **q** and branch λ. Then the relevant Hamiltonian is given by

$$H = \hbar\omega_{q\lambda}(b^{\dagger}_{q\lambda}b_{q\lambda} + 1/2) + \sum_{i,k} E_i^{(0)} C^{\dagger}_{ik} C_{ik} + \sum_{i,jk}[\, D_{ij}(k,q\lambda) C^{\dagger}_{ik+q} C_{jk} b_{q\lambda} + (h.c.)], \tag{A3.1}$$

where $C^{\dagger}_{ik}(C_{ik})$ denotes the creation(annihilation) operator of the electron having wavevector **k** and energy $E_i^{(0)}$ and $b^{\dagger}_{q\lambda}(b_{q\lambda})$ the Boson operator of the phonon with frequency $\omega_{q\lambda}$. The coupling constant $D_{ij}(k,q\lambda)$ strongly depends on Bloch states. So that its dependence on electronic states should be correctly taken into consideration. The lattice distortion corresponding to the phonon mode defines the new Boson operator

$$B_{q\lambda} = b_{q\lambda} - b, \tag{A3.2}$$

with

$$b = -\sum_{i,jk} D^{*}_{ij}(k,q\lambda) \langle C^{\dagger}_{ik+q} C_{jk} \rangle^{*} / (\hbar\omega_{q\lambda}), \tag{A3.3}$$

where $\langle \cdots\cdots \rangle$ means the thermal average over the whole system. Eq. (A3.2) suggests that the normal coordinate for this phonon mode shifts the vibrational center to the amount of

$$\delta r(q\lambda) = (2\hbar/\omega_{q\lambda})^{1/2}\, b. \tag{A3.4}$$

An atomic displacement of the μth atom in the ith unit cell is given by

$$\vec{\delta r}(\mu,i) = (NM_{\mu})^{-1/2}\, \vec{\varepsilon}(q\lambda,\mu)\, \delta r(q\lambda)\, \exp(iq\cdot R_i), \tag{A3.5}$$

where $\vec{\varepsilon}(q\lambda,\mu)$ is the polarization vector for the μth atom of mass M_{μ}, R_i the position vector of the ith unit cell, and N the number of unit cells. Using Eqs.(A3.2), (A3.3), and (A3.4), we obtain the transformed Hamiltonian

$$H = H_0 + H',$$

$$H_0 = \hbar\omega_{q\lambda}(B^{\dagger}_{q\lambda}B_{q\lambda} + 1/2) + \omega_{q\lambda}\delta r(q\lambda)^2/2 + \sum_{i,k} E_i^{(0)} C^{\dagger}_{ik} C_{ik}$$
$$+ \sum_{i,jk}[\delta r(q\lambda)(\omega_{q\lambda}/2\hbar)^{1/2}\, D_{ij}(k,q\lambda) C^{\dagger}_{ik+q} C_{jk} + (h.c.)], \tag{A3.6}$$

$$H' = \sum_{i,jk}[D_{ij}(k,q\lambda)(C^{\dagger}_{ik+q}C_{jk} - \langle C^{\dagger}_{ik+q}C_{jk}\rangle)B_{q\lambda} + (h.c.)]. \tag{A3.7}$$

In the mean field approximation H' vanishes and band energies in a distorted lattice are obtained by diagonalizing the last two terms in H_0. So the energy eigenvalue is written to first order

in $\delta r(q\lambda)$ as follows:

$$E_{ik} = E_i^{(0)} + \delta r(q\lambda)\ g_{ik}(q\lambda), \tag{A3.8}$$

where i specifies a subband and k is taken in the Brillouin zone for the distorted lattice. $g_{ik}(q\lambda)$ is a function of $D_{ij}(k,q\lambda)$, $D_{ij}(k\pm q,q\lambda)$etc..

In the mean field approximation, the free energy is calculated with the use of the unperturbed Hamiltonian H_0 and expressed as

$$F = \omega_{q\lambda}^{\ 2}\ \delta r(q\lambda)^2/2 + \mu N_{el}$$
$$- k_B T \sum_{i,k} \ln[1 + \exp\{(\mu - E_{ik})/(k_B T)\}], \tag{A3.9}$$

where μ is the chemical potential, and N_{el} the number of electrons, and E_{ik} is given by Eq. (A3.8). Here the contributions of the lattice viblation are omitted other than the increase of the elastic energy expressed in the first term in Eq. (A3.9). So that the elasticity constant c introduced in Eq. (4.2) of the text is related to the phonon frequency $\omega_{q\lambda}$. With the aid of the group theoretical consideration given in Appendix 4, we find that the three types of lattice distortion discussed in §3 correspond to an optical phonon mode at the zone-center, which belongs to doubly degenerate E_g representation. Thus, using Eq.(A3.5) and neglecting the displacement of Cl ions, we have for a Ti ion $|\vec{\varepsilon}(q=0, E_g)| = 1/\sqrt{2}$ and obtain the relation

$$c = 2NM\omega_0^2, \qquad \text{(A3.10)}$$

where ω_0 represents the frequency of the E_g mode at Γ point, and M the mass of Ti ion, and N is the number of unit cells.

Next we calculate the intraband elements in the tight-binding approximation. Using the folding down method of the seqular eqation, we obtain the effective matrix for the 3dε Bloch states in the distorted structure. It is of infinite dimension except for the case of a commensurate distortion, and is written in the form

$$K_{dd}^{eff}(E,k;q\lambda) =$$

$$\begin{array}{c} \\ \vdots \\ \{\Psi(k-q)\} \\ \{\Psi(k)\} \\ \{\Psi(k+q)\} \\ \vdots \end{array} \begin{array}{c} \cdots \quad \{\Psi(k-q)\} \qquad\qquad \{\Psi(k)\} \qquad\qquad \{\Psi(k+q)\} \quad \cdots \\ \left[\begin{array}{ccc} K_{dd}^0(E) & \Delta K_{dd}(k-q,k;E) & 0 \\ \Delta K_{dd}(k,k-q;E) & K_{dd}^0(E) & \Delta K_{dd}(k,k+q;E) \\ 0 & \Delta K_{dd}(k+q,k;E) & K_{dd}^0(E) \\ \vdots & \vdots & \vdots \end{array}\right] \end{array}$$

$$\text{with} \quad \Delta K_{dd}(k,k+q;E) = \{(\gamma-ES)/E\}\delta r(q\lambda)\, M'_{dd}(k,k+q,\lambda;E) \text{ etc.}, \qquad \text{(A3.11)}$$

where $\delta r(q\lambda)$ represents the normal coordinate for the lattice viblational mode, and $\{\Psi(k)\}$ means the six 3d Bloch functions in the undistorted phase given by Eq. (2.17) of the text, and $K_{dd}^0(E)$

is also given by Eq. (2.11). The intraband elements of $M'_{dd}(k,k+q,\lambda;E)$ are written as follows:

$$M'_{dd}(k,k+q,\lambda;E) = \tag{A3.12}$$

$$\begin{array}{c} \\ \Psi_{1+}(k) \\ \Psi_{2a+}(k) \\ \Psi_{2b+}(k) \\ \Psi_{1-}(k) \\ \Psi_{2a-}(k) \\ \Psi_{2b-}(k) \end{array} \begin{array}{c} \begin{array}{cccccc} \Psi_{1+}(k+q) & \Psi_{2a+}(k+q) & \Psi_{2b+}(k+q) & \Psi_{1-}(k+q) & \Psi_{2a-}(k+q) & \Psi_{2b-}(k+q) \end{array} \\ \begin{pmatrix} M_+ & & & & & \\ & M_+^{aa} & M_+^{ab} & & & \\ & (M_+^{ab})^* & M_+^{bb} & & & \\ & & & M_- & & \\ & & & & M_-^{aa} & M_-^{ab} \\ & & & & (M_-^{ab})^* & M_-^{bb} \end{pmatrix} \end{array}$$

where each element is a function of $\mathbf{k}$, $\mathbf{q}$, and E, and also depends on the additional tight-binding parameters S', γ' etc. and the polarization vector $\vec{\varepsilon}(q\lambda,\mu)$ of the μth Ti ion (μ=I,II). After some laborious calculation, we obtain the explicit expression of the intraband element as given in Table A3.

Table A3. Generalized expression of intraband element

$$\pm\Delta(E)[(\varepsilon_{IX}/\sqrt{6})\ f_X\{-(q_a-\theta-\phi,\ q_b+\theta-\phi) - (\phi-\theta,\theta) - 2(q_a+\theta+\phi,\ q_b-\theta)\}$$

$$+(\varepsilon_{IY}/\sqrt{2})\ f_Y\{-(q_a-\theta-\phi,\ q_b+\theta-\phi) + (\phi-\theta,\theta)\}$$

$$+(\varepsilon_{IIX}/\sqrt{6})\ f_X\{-(q_a-\theta+\phi,\ q_b+\theta+\phi) + 2(-\phi-\theta,\theta) + (q_a+\theta-\phi,\ q_b-\theta)\}$$

$$+(\varepsilon_{IIY}/\sqrt{2})\ f_Y\{(q_a-\theta+\phi,\ q_b+\theta+\phi) - (q_a+\theta-\phi,\ q_b-\theta)\}]$$

$$+\Delta(E)[(\varepsilon_{IIX}/\sqrt{6})\ f_X\{3(q_{ab}+\phi,\ -q_{ab}) - (q_a+\phi,\ q_b) + (q_a-\phi,q_b-\phi) + 2(0,\phi)\}$$

$$+(\varepsilon_{IIY}/\sqrt{2})\ f_Y\{-(q_{ab}+\phi,\ -q_{ab}) + (q_a+\phi,\ q_b) - (q_a-\phi,\ q_b-\phi) + (q_a+q_b-\phi,\ q_a+q_b-\phi)\}]$$

$$\pm\sigma(E)[(\varepsilon_{IX}/\sqrt{6})\ f_X\{-(k_a+q_b+\theta-\phi,\ k_b+q_a-\theta-\phi) + (k_{ab}-\theta+\phi,\ -k_{ab}+\theta) - 3(k_{ab}+k_a+q_a,\ -k_{ab}+k_b+q_b+\phi) + 2(-k_a+q_a+\theta+\phi,\ -k_a+q_b-\theta)\}$$

$$+(\varepsilon_{IY}/\sqrt{2})\ f_Y\{(k_a+q_b+\theta-\phi,\ k_b+q_a-\theta-\phi) - (k_{ab}-\theta+\phi,\ -k_{ab}+\theta) - (k_{ab}+k_a+q_a,\ -k_{ab}+k_b+q_b+\phi) + (-k_a-k_b-\phi,\ -k_a-k_b-\phi)\}$$

$$+(\varepsilon_{IIX}/\sqrt{6})\ f_X\{-(-k_b+\theta+\phi,\ -k_a-\theta+\phi) + (k_{ab}+q_a-\theta,\ -k_{ab}+q_b+\theta-\phi) - 3(k_{ab}-k_b+q_{ab}-\phi,\ -k_{ab}-k_a-q_{ab}) + 2(k_a+q_a+\theta,\ k_b+q_b-\theta-\phi)\}$$

$$+(\varepsilon_{IIY}/\sqrt{2})\ f_Y\{-(-k_b+\theta+\phi,\ -k_a-\theta+\phi) + (k_{ab}+q_a-\theta,\ -k_{ab}+q_b+\theta-\phi) + (k_{ab}-k_b+q_{ab}-\phi,\ -k_{ab}-k_a-q_{ab}) - (k_a+k_b+q_a+q_b+\phi,\ k_a+k_b+q_a+q_b+\phi)\}]$$

$$\pm\Pi(E)[(\varepsilon_{IX}/\sqrt{6})\ f_X\{-(k_{ab}+q_a,\ -k_{ab}+q_b+\phi) + (-k_b-\phi,\ -k_a-\phi)$$

$$- 2(k_a+q_a, k_b+q_b+\phi)\}$$

$$+(\varepsilon_{IY}/\sqrt{2})\ f_Y\{-(k_{ab}+q_a,\ -k_{ab}+q_b+\phi) + (-k_b-\phi,\ -k_a-\phi)\}$$

$$+(\varepsilon_{IIX}/\sqrt{6})\ f_X\{-(k_{ab}+q_a-\phi,\ -k_{ab}+q_b) - 2(-k_b-\phi,\ -k_a)$$

$$+ (k_a+q_a+\phi,\ k_b+q_b+\phi)\}$$

$$+(\varepsilon_{IIY}/\sqrt{2})\ f_Y\{(k_{ab}+q_a-\phi,\ -k_{ab}+q_b) - (k_a+q_a+\phi,\ k_b+q_b+\phi)\}]$$

$$+\Pi(E)[(\varepsilon_{IIX}/\sqrt{6})\ f_X\{(k_a+q_a-\theta+\phi,\ k_b+q_b+\theta) - (k_a+q_b-\theta+\phi,\ k_b+q_a+\theta)$$

$$+ (k_{ab}+\theta-\phi,\ -k_{ab}-\theta-\phi) + (k_{ab}+q_a+\theta-\phi,\ -k_{ab}+q_b-\theta-\phi)$$

$$+ 2(-k_b+q_a-\theta,\ -k_a+q_b+\theta+\phi) - 2(-k_b-\theta,\ -k_a+\theta+\phi)\}$$

$$+(\varepsilon_{IIY}/\sqrt{2})\ f_Y\{-(k_a+q_a-\theta+\phi,\ k_b+q_b+\theta) + (k_a+q_b-\theta+\phi,\ k_a+q_a+\theta)$$

$$- (k_{ab}+\theta-\phi,\ -k_{ab}-\theta-\phi) + (k_{ab}+q_a+\theta-\phi,\ -k_{ab}+q_b-\theta-\phi)\}]$$

where $k_{ab} = k_a - k_b$, $\quad q_{ab} = q_a - q_b$, and

$$f_X(k_a,\ k_b) = (1/6)[\exp(ik_a) - \exp(ik_b)],$$

$$f_Y(k_a,\ k_b) = (1/6)[\exp(ik_a) + \exp(ik_b)].$$

The addition or the subtraction of the form

$$f_\alpha(a_1,b_1) \pm f_\alpha(a_2,b_2) \pm \cdots\cdots \pm f_\alpha(a_i,b_i) \qquad (\alpha = X,Y)$$

is written as follows:

$$f_{\alpha}\{(a_1,b_1) \pm (a_2,b_2) \pm \cdots\cdots \pm (a_i,b_i)\}.$$

Here a wavevector is written as

$$\mathbf{k} = (k_a \mathbf{a}^* + k_b \mathbf{b}^*)/(2\pi),$$

and a polarization vector of the μth Ti ion (μ=I,II) as

$$\boldsymbol{\varepsilon}(\mathbf{q}\lambda,\mu) = \varepsilon_{\mu X} \mathbf{X} + \varepsilon_{\mu Y} \mathbf{Y},$$

where **X** and **Y** are unit vectors in the X and Y directions, respectively shown in Fig. 2-2 in the text.

We set

$\theta = \phi = 0$ for M_+ and M_-,

$\theta = 2\pi/3, \quad \phi = 0$ for M_+^{aa} and M_-^{aa},

$\theta = -2\pi/3, \quad \phi = 0$ for M_+^{bb} and M_-^{bb},

$\theta = 0, \quad \phi = 2\pi/3$ for M_+^{ab} and M_-^{ab},

$\theta = 0, \quad \phi = -2\pi/3$ for M_+^{ba} and M_-^{ba},

and take the upper or the lower in the double sign according to the sign in the suffix of M.

Appendix 4. Lattice Vibrational Mode

We show in Fig. A4-1 the two-dimensional Brillouin zone for the undistorted lattice of $TiCl_3$. The unit cell of the sandwich structure contains two Ti^{3+} ions and six Cl^- ions. So there are twentyfour normal modes of the lattice vibration. In Table A4 we list the irreducible representation of the normal mode at the symmetry point in the Brillouin zone together with its point group. From the group theoretical consideration we also obtain a basis set of symmetrical coordinates that reduces a dynamical matrix to submatrices according to the irreducible representation. The symmetrical coordinate is constructed from the displacements either of Ti ions or of Cl ions The vibrational patterns expected from the symmetrical coordinate are summarized as follows:

Γ point modes

A_{1g} modes; expansive or compressive vibrations of Cl ions parallel and perpendicular to their sheets. (These two modes are normal modes.)

A_{2g} modes; vibration of Ti ions perpendicular to their sheet, and shear mode of Cl's parallel to their sheets.

E_g modes; two kinds of independent vibration of Ti ions discussed in §§3 and 4, and six kinds of Cl ions' mode, the four being parallel to their sheets (see Fig. A4-2) and the two perpendicular to them.

Here we considered the even parity modes only.

M point modes

The periodicity of these vibrational modes is two times larger than the basis periodicity in the direction of either or both of the basis vectors.

A_g modes; one kind of Ti ions' vibration parallel to their sheet shown in Fig. A4-3, and five kinds of complex vibration of Cl ions.

B_g modes; similar to A_g modes but the direction of ionic displacement rotated by 90° around the c-axis.

When two Ti ions in the unit cell move against each other, the lattice distortion of this type is described by the normal coordinate for the phonon modes considered here, because inversion symmetry is preserved only at Γ and M points. For this reason and by reference to the conjecture found by Ogawa and Emeis et al. we examined only the even parity phonon modes in this Appendix.

Table A4. Irreducible representation of phonon mode

symmetry point	point group	irreducible representation of normal phonon mode
Γ	D_{3d}	$2A_{1g} + 2A_{2g} + 4E_g + A_{1u} + 3A_{2u} + 4E_u$
K	C_{3v}	$5A_1 + 3A_2 + 8E$
M	C_{2h}	$6A_g + 6B_g + 5A_u + 7B_u$
Σ	C_2	11A + 13B
T, T'	C_s	11A + 13B

Figure captions

Fig. A4-1. Two-dimensional Brillouin zone for the sandwich structure.

Fig. A4-2. The symmetrical coordinates of Cl ions for Γ point E_g mode. Another two coordinates are obtained by rotating the coordinates shown in the figure about the two-fold Y axis.

Fig. A4-3. The displacement of Ti ions corresponding to M point A_g mode having wavevector $\mathbf{a}^*/2$ (a) and $(\mathbf{a}^* + \mathbf{b}^*)/2$ (b).

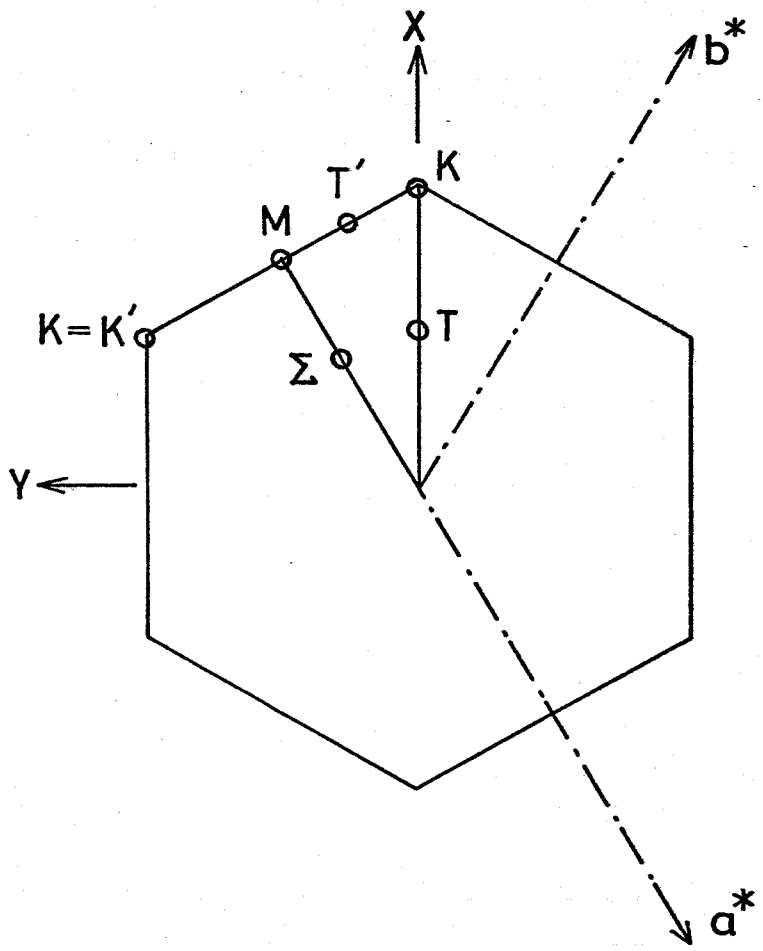

Fig. A4-1

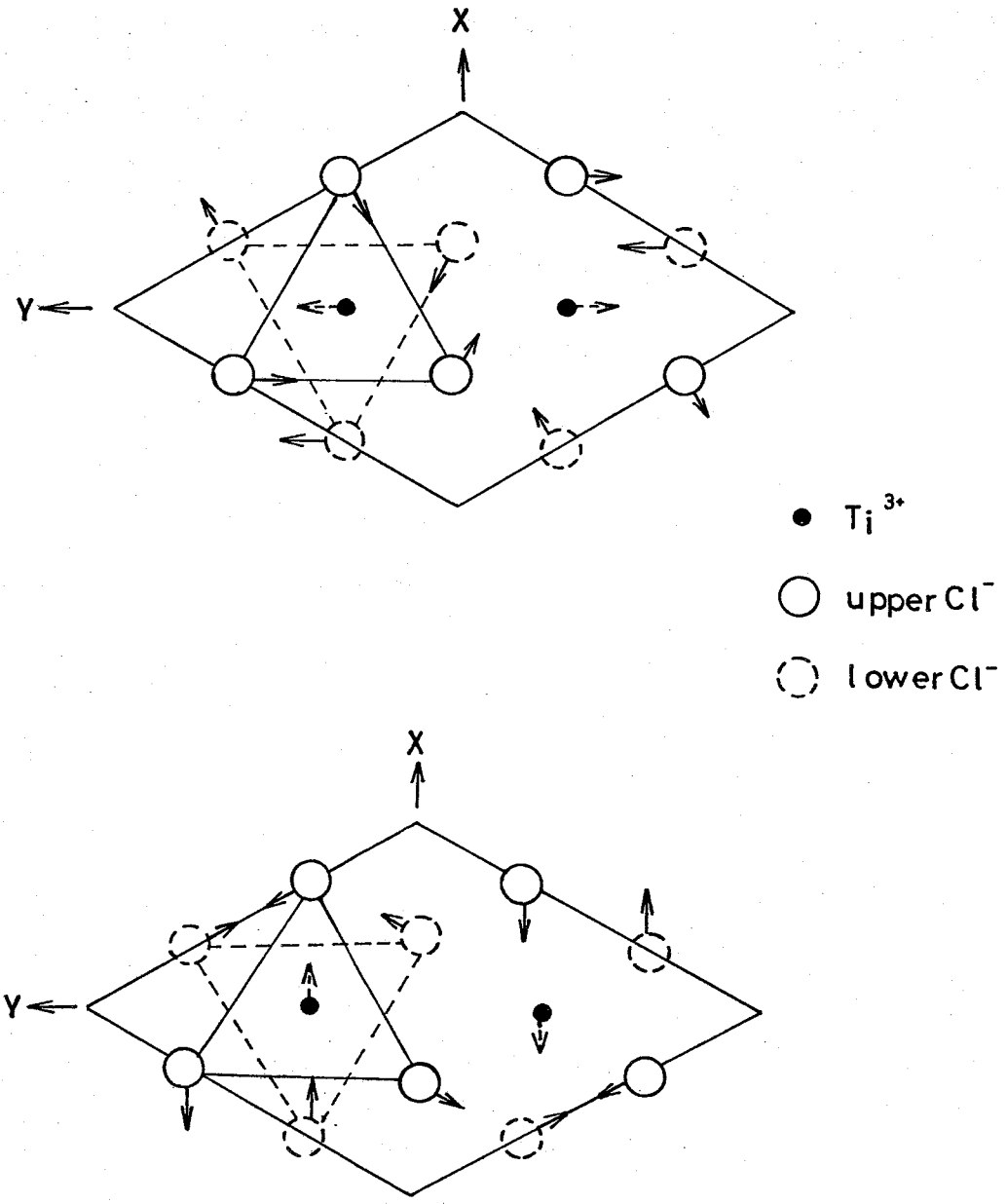

Fig. A4-2

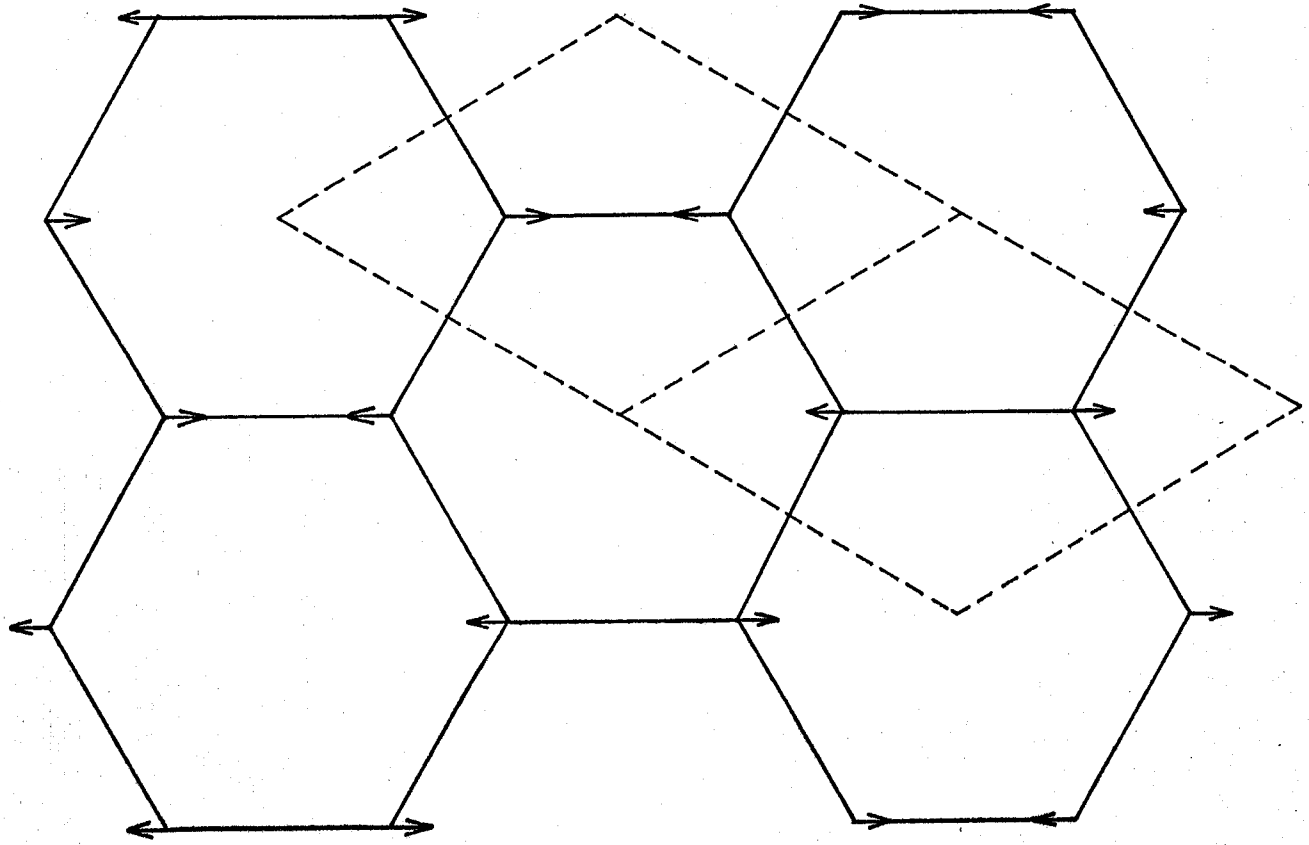

Fig. A4-3a

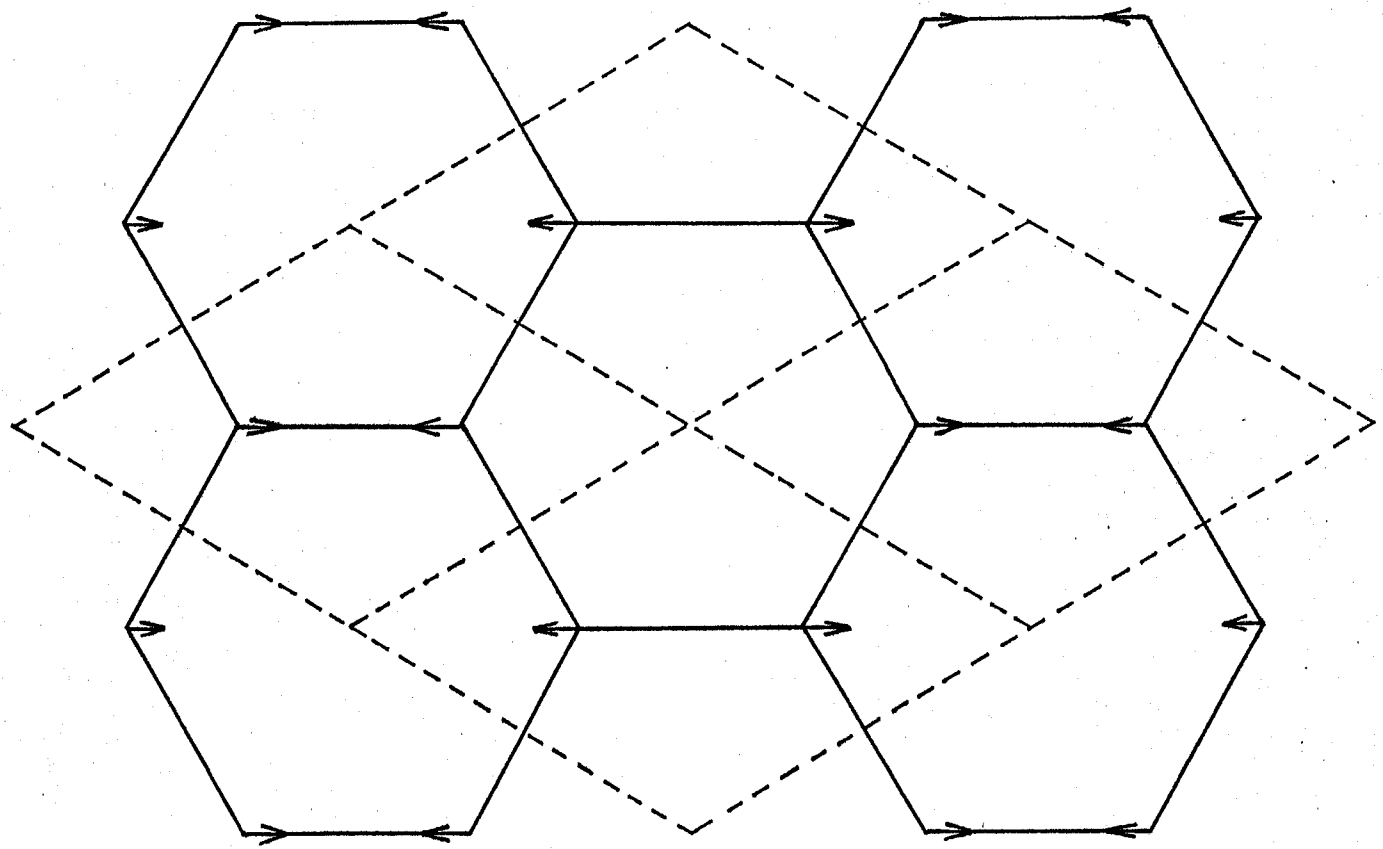

Fig. A4-3b

Appendix 5. Lattice Distortion Corresponding to M Point Mode

Here we consider the three dε bands having lower energies in the undistorted phase and their intraband elements. The effective matrix K_{dd}^{eff} for M point modes is written in the form

$$K_{dd}^{eff}(E,k,Q) = \tag{A5.1}$$

$$\begin{array}{c} \\ \Psi_{1-}(k) \\ \Psi_{1-}(k+Q) \\ \Psi_{2a+}(k) \\ \Psi_{2b+}(k) \\ \Psi_{2a+}(k+Q) \\ \Psi_{2b+}(k+Q) \end{array}
\begin{array}{c}
\begin{array}{cccccc} \Psi_{1-}(k) & \Psi_{1-}(k+q) & \Psi_{2a+}(k) & \Psi_{2b+}(k) & \Psi_{2a+}(k+Q) & \Psi_{2b+}(k+Q) \end{array} \\
\left[\begin{array}{cccccc}
\varepsilon_{dp}-E & \delta rM_{-}\times & & & & \\
+2\Delta_0^2/E & \Delta_0/E & & & & \\
\delta rM_{-}^{*} & \varepsilon_{dp}-E & & & & \\
\times\Delta_0/E & +2\Delta_0^2/E & & & & \\
 & & \varepsilon_{dp}-E & & \delta rM_{+}^{aa} & \delta rM_{+}^{ab} \\
 & & +3\Delta_0^2/E & 0 & \times\Delta_o/E & \times\Delta_0/E \\
 & & & \varepsilon_{dp}-E & \delta rM_{+}^{ba} & \delta rM_{+}^{bb} \\
 & & 0 & +3\Delta_0^2/E & \times\Delta_0/E & \times\Delta_0/E \\
 & & \delta rM_{+}^{aa*} & \delta rM_{+}^{ba*} & \varepsilon_{dp}-E & \\
 & & \times\Delta_0/E & \times\Delta_0/E & +3\Delta_0^2/E & 0 \\
 & & \delta rM_{+}^{ab*} & \delta rM_{+}^{bb*} & & \varepsilon_{dp}-E \\
 & & \times\Delta_0/E & \times\Delta_0/E & 0 & +3\Delta_0^2/E
\end{array}\right],
\end{array}$$

with $\Delta_0(E) = \gamma - ES$,

where M_-, M_+^{aa} etc. of the nondiagonal elements depend on k, Q(= $\pm a^*/2$, $\pm b^*/2$, $\pm(a^* + b^*)/2$) and E, and they are derived from Table A3 in Appendix 3, and δr stands for the normal coordinate for M point phonon modes.

In §2 of the text we have obtained the following relation:

$$\varepsilon_{dp} + (m+1)\Delta_0^2(E)/E - E \qquad \text{(A5.2)}$$

$$= - \{1 - (m+1)S^2\}(E - E_{dm})(E - E_{pm})/E, \qquad (m=1,2,2)$$

where

$$E_{dm} = \frac{1}{2\{1-(m+1)S^2\}} [\varepsilon_{dp} - 2(m+1)\gamma S + \sqrt{(\varepsilon_{dp})^2 + 4(m+1)\gamma\Delta_0(\varepsilon_{dp})}],$$

E_{pm} = similar to the above with - in front of the square root.

So E_{d1} and E_{d2} are energy eigenvalues in the undistorted phase for the first singlet and first doublet, respectively. If we take only the intraband elements and use Eq. (A5.2), the seqular equation

$$\det\left| K_{dd}^{eff}(E,k,Q)\right| = 0$$

is reduced to the following two equations:

$$\det \begin{vmatrix} E_{d1} - E & \delta r y_1(E) M_+^*(E) \\ \delta r y_1(E) M_+^*(E) & E_{d1} - E \end{vmatrix} = 0, \qquad \text{(A5.3a)}$$

$$\det \begin{vmatrix} E_{d2} - E & 0 & \delta r y_2(E) M_+^{aa}(E) & \delta r y_2(E) M_+^{ab}(E) \\ 0 & E_{d2} - E & \delta r y_2(E) M_+^{ba}(E) & \delta r y_2(E) M_+^{bb}(E) \\ \delta r y_2(E) M_+^{aa}(E)^* & \delta r y_2(E) M_+^{ba}(E)^* & E_{d2} - E & 0 \\ \delta r y_2(E) M_+^{ab}(E)^* & \delta r y_2(E) M_+^{bb}(E)^* & 0 & E_{d2} - E \end{vmatrix} = 0,$$

(A5.3b)

where

$$y_m(E) = \Delta_0(E)/[(1 - (m+1)S^2)(E - E_{pm})], \quad (m=1,2).$$

If we consider the energy correction only to first order in δr, we can, as is easily verified, replace the variable E in the non-diagonal elements (in Eq.(A5.3)) with the energy E_{d1} or E_{d2} in the undistorted phase according to the band relevant to the equation. In this approximation, the eigenvalue problem given by the secular equation (A5.3) is reduced to the usual one of the diagonalization of Hamiltonian. And then the nondiagonal elements can be regarded as the intraband mixing elements that arise through the electron-phonon interaction. Namely, we obtain the effective Hamiltonian for the six Bloch states as follows:

$$H_{dd}^{eff} =$$

$$
\begin{array}{c}
 \\
\Psi_{1-}(k) \\
\Psi_{1-}(k+Q) \\
\Psi_{2a+}(k) \\
\Psi_{2b+}(k) \\
\Psi_{2a+}(k+Q) \\
\Psi_{2b+}(k+Q)
\end{array}
\begin{array}{c}
\begin{array}{cccccc}
\Psi_{1-}(k) & \Psi_{1-}(k+Q) & \Psi_{2a+}(k) & \Psi_{2b+}(k) & \Psi_{2a+}(k+Q) & \Psi_{2b+}(k+Q)
\end{array} \\
\left(\begin{array}{cccccc}
E_{d1} & \delta r M_1 & & & & \\
\delta r M_1^* & E_{d1} & & & & \\
 & & E_{d2} & 0 & \delta r M_a & \delta r M_{ab} \\
 & & 0 & E_{d2} & \delta r M_{ba} & \delta r M_b \\
 & & \delta r M_a^* & \delta r M_{ba}^* & E_{d2} & 0 \\
 & & \delta r M_{ab}^* & \delta r M_b^* & 0 & E_{d2}
\end{array}\right)
\end{array}
, \qquad \text{(A5.4)}
$$

where

$$M_1 = M_+(k,Q;E_{d1})\Delta_0(E_{d1})/[(\varepsilon_{dp})^2 + 8\gamma\Delta_0(\varepsilon_{dp})]^{1/2},$$

$$M_a = M_+^{aa}(k,Q;E_{d2})\Delta_0(E_{d2})/[(\varepsilon_{dp})^2 + 12\gamma\Delta_0(\varepsilon_{dp})]^{1/2},$$

$$M_b = M_+^{bb}(k,Q;E_{d2})\Delta_0(E_{d2})/[(\varepsilon_{dp})^2 + 12\gamma\Delta_0(\varepsilon_{dp})]^{1/2},$$

$$M_{ab} = M_+^{ab}(k,Q;E_{d2})\Delta_0(E_{d2})/[(\varepsilon_{dp})^2 + 12\gamma\Delta_0(\varepsilon_{dp})]^{1/2},$$

$$M_{ba} = M_+^{ba}(k,Q;E_{d2})\Delta_0(E_{d2})/[(\varepsilon_{dp})^2 + 12\gamma\Delta_0(\varepsilon_{dp})]^{1/2},$$

and δr stands for the normal coordinate for the lattice vibrational mode specified by wavevector $\mathbf{Q}$.

The six eigenvalues of H_{dd}^{eff} are obtained as follows:

$$E_{d1} \pm \delta r|M_1|,$$

$$E_{d2} \pm \delta r/\sqrt{2}[G_1 + (G_2^2 + G_3^2)^{1/2}]^{1/2}, \qquad \text{(A5.5)}$$

and $$E_{d2} \pm \delta r/\sqrt{2}[G_1 + (G_2^2 - G_3^2)^{1/2}]^{1/2},$$

where

$$G_1 = |M_a|^2 + |M_b|^2 + |M_{ab}|^2 + |M_{ba}|^2,$$

$$G_2 = |M_a|^2 - |M_b|^2 + |M_{ab}|^2 + |M_{ba}|^2,$$

and $$G_3 = 2|M_a M^*_{ab} + M_{ba} M^*_a|.$$

So that, from the coefficient of δr in Eq. (A5.5) (including the sign), we obtain the explicit expression of $g_{ik}(Q\lambda)$ introduced in §3 of the text.

List of Publications

1. K. Motizuki and S. Miyata: Temperature Dependence of Two-Exciton Transitions in $RbMnF_3$ and MnF_2. Solid State Commun. 11, 167 (1972).

2. S. Miyata and K. Motizuki: Cluster Approach to Magnon Raman Scattering in Cubic Antiferromagnet. J. Phys. Soc. Japan 38, 1020 (1975).